GATA1-defective immune-megakaryocytes as possible drivers of idiopathic pulmonary fibrosis

Francesca Gobbo[1,3*], Maria Zingariello[2*], Paola Verachi[3], Mario Falchi[4], Francesca Arciprete[2], Fabrizio Martelli[5], Angelo Peli[6], Maria Mazzarini[3,7], Jeff Vierstra[7], Carolyn Mead-Harvey[8], Amylou C. Dueck[8], Giuseppe Sarli[1], Stefano Nava[9,10], Giacomo Sgalla[11], Luca Richeldi[11] and Anna Rita Migliaccio[2,7]

[1]Department of Veterinary Medical Sciences, University of Bologna, Ozzano dell'Emilia (Bologna) 40064, Italy; [2]Unit of Microscopic and Ultrastructural Anatomy, Department of Medicine, University Campus Bio-Medico, Rome 00128, Italy; [3]Department of Biomedical and Neuromotor Sciences, University of Bologna, Bologna, Italy; [4] National Center HIV/AIDS Research, Istituto Superiore di Sanità, Rome 00161, Italy; [5]National Center for Preclinical and Clinical Research and Evaluation of Pharmaceutical Drugs, Istituto Superiore di Sanità, Rome 00161, Italy; [6]Department for Life Quality Studies, University of Bologna, Rimini Campus, Rimini 47921, Italy; [7]Altius Institute for Biomedical Sciences, Seattle, WA 98121, USA; [8]Mayo Clinic, Department of Quantitative Health Sciences, Division of Clinical Trials and Biostatistics, Scottsdale, AZ 85259, USA; [9]IRCCS Azienda Ospedaliero-Universitaria di Bologna, Respiratory and Critical Care Unit, Bologna 40138, Italy; [10] Department of Medical and Surgical Sciences, University of Bologna, Bologna 40138, Italy; [11]Department of Medical and Surgical Sciences Fondazione Policlinico Universitario "A. Gemelli" IRCCS, Università Cattolica del Sacro Cuore, Roma 00168, Italy.

* denotes equal contribution

Corresponding Author: Anna Rita Migliaccio, Altius Institute for Biomedical Sciences, Seattle, WA, USA. amigliaccio@altius.org

Word counts: Title: 10 words (max:10-12 words and 150 characters including spaces), abstract: 147 words (max: n. 150 words), text **8445** words (max: n. 7000 words from title to figure legend excluding refs, STAR Methods and supplemental legend and refs), references: **70** (max n. 50)+ **9 refs M&M**, Figures 6 + 1 Table (7 as max). **10** Supplementary Figures + 3 supplementary Tables (plus 2 links for a total of 12 movies on Zenodo) for a total of **15 items for a max of 7.**

Summary

Idiopathic pulmonary fibrosis (IPF) is a progressive fibrotic lung disorder with limited therapeutic options. Insufficient understanding of driver mutations and poor fidelity of currently available animal models has limited the development of effective therapies. Since GATA1deficient megakaryocytes sustain myelofibrosis, we hypothesized that they may also induce fibrosis in lungs. We discovered that lungs from IPF patients and *Gata1*^{low} mice contain numerous GATA1negative immune-poised megakaryocytes that, in mice, have defective RNA-seq profiling and increased TGF-β1, CXCL1 and P-selectin content. With age, *Gata1*^{low} mice develop fibrosis in lungs. Development of lung fibrosis in this model is prevented by *P-selectin* deletion and rescued by P-selectin, TGF-β1 or CXCL1 inhibition. Mechanistically, P-selectin inhibition decreases TGF-β1 and CXCL1 content and increases GATA1positive megakaryocytes while TGF-β1 or CXCL1 inhibition decreased CXCL1 only. In conclusion, *Gata1*^{low} mice are the first genetic-driven model for IPF and provide a link between abnormal immune-megakaryocytes and lung fibrosis.

Keywords

Idiopathic pulmonary fibrosis, megakaryocytes, GATA1, TGF-β, P-selectin, CXCL1.

Highlights

- Lungs from IPF patients contain many GATA1 negative immune MK
- *Gata1*^{low} mice are the first genetic model with a pathophysiology similar to IPF
- *Gata1*^{low} lungs mice contain defective immune MK with high P-sel, TGF-β and CXCL1
- *P-sel* ablation or P-sel/TGF-β/CXCL1 inhibition rescues fibrosis in *Gata1*^{low} lung

55 **Introduction**

56 Idiopathic pulmonary fibrosis (IPF) is a chronic, progressive form of pneumonia associated with
57 fibrosis of unknown etiology[1]. IPF represents the prototypic form of progressive pulmonary
58 fibrosis (PPF), also associated with other non-idiopathic conditions. IPF occurs primarily in older
59 adults (usually >60 years of age) and leads to progressive deterioration of pulmonary function, and
60 eventual death from chronic or acute respiratory failure[1,2]. Its incidence is 3-9 cases every 100,000
61 inhabitants and manifests itself prevalently in males with known risk factors such as smoking[3].
62 Studies of IPF and PPF pathobiology are hampered by limited availability of lung biopsies due to
63 the fact that lung biopsy is no longer needed for diagnosis. While animal models of IPF/PPF have
64 been proposed, the fidelity between the human disease and the currently available models is poor.
65 Current animal models employed to study the pathobiology and to identify candidate treatments
66 for IPF are animals (usually mice or rats) forced to breath bleomycin[4], a chemotherapeutic
67 compound that has lung toxicity as its major adverse effect[5]. Animals subjected to bleomycin
68 develop acute inflammation and fibrosis in the lungs which eventually leads to their death within
69 one-two weeks. In spite of its widespread use, bleomycin has several limitations which reduce its
70 clinical relevance. First, the aggressive progression of fibrosis in this model does not resemble that
71 of IPF, where fibrosis develops slowly over many years. Second, IPF usually affects individuals
72 without previous exposures to chronic inflammatory insults, suggesting that inflammation
73 represents a confounding factor in translating the results from these models to humans. Third and
74 most importantly, the lesions developed in this model are associated with acute alveolar damage,
75 including edema, and have a bronchiolo-centric localization, likely the consequence of the intra-
76 tracheal route of the drug administration[6]. By contrast, in IPF fibrosis occurs mostly in the basal
77 lobes of the lung, is predominantly subpleural, and tends to extend to the para-septal parenchyma
78 generating the typical honeycomb pattern revealed by high-resolution computed tomography
79 (HRCT) of the chest[7]. Such different anatomic localization strongly suggests that the cells
80 responsible for fibrosis in the animal models and in IPF patients are different. Nevertheless, studies
81 in bleomycin mice, validated by observations in patients, have implicated abnormally high levels
82 of several pro-fibrotic proteins, such as transforming growth factor-β (TGF-β)[8], interleukin-8 (IL-
83 8)[9], and the adhesion receptor P-selectin (P-SEL)[10], among others, in the etiology of IPF. In the
84 case of TGF- β, the availability of chemical inhibitors[11] and validation experiments demonstrating
85 that mice forced to breath adenoviruses containing TGF-β develop fibrosis in the lung[12,13], have

86 inspired clinical trials with pirfenidone and nintedanib, two pleiotropic proinflammatory inhibitors
87 also targeting TGF-β, in IPF[14–17]. However, these two drugs have been shown to be effective in
88 slowing down the decline of lung function, but not in preventing disease progression in most IPF
89 patients[14–17]. Therefore, the only cure for IPF is lung transplantation, an option available to only a
90 limited number of patients[1–3]. The clinical needs of IPF patients highlight the need for novel,
91 possibly genetically driven, animal models which more closely resemble the pathological
92 mechanisms of IPF in patients. It is conceivable that these models may also shed light on the
93 genetic drivers for IPF which are still largely unknown. In fact, although familial clustering and
94 association studies suggest that the disease has a genetic basis[3,18], a causative genetic link is yet to
95 be established. The identification that loss-of-function mutations in the *telomerase* gene[19], or in
96 genes, such as *ZCCH8*, which encode proteins required for expression of the *telomerase*[20], in
97 patients with familiar IPF raised great hope that the genetic cause of the disease had been finally
98 discovered[21]. However, induction of telomerase-deficiency in mice increases the senescence of
99 both hematopoietic and alveolar stem cells but the mice, although more susceptible to bleomycin-
100 induced lung fibrosis, do not develop IPF at baseline[22,23].

101 Recent experiments have demonstrated that activation of *c-Jun*, a gene downstream to TGF-β,
102 induces fibrosis in multiple organs, including bone marrow (BM) and lung, in mice[24,25]. In the case
103 of myelofibrosis (MF), the most severe of the Philadelphia-chromosome negative
104 myeloproliferative neoplasms[26,27], c-jun is activated by increased microenvironment
105 bioavailability of TGF-β produced by abnormal megakaryocytes[28,29]. In fact, the MK in the BM
106 of patients with myelofibrosis remain immature due to a RSP14 ribosomopathy induced by the
107 driver mutations that reduces the translation of the mRNA for GATA1[30,31], the transcription factor
108 essential for their proper maturation[32]. The causative role of this abnormal MK in the etiology of
109 the disease has been validated by experiments demonstrating that mice expressing either the driver
110 mutations or low levels of *Gata1* (*Gata1^{low} mice)* only in MK[33] develop myelofibrosis with age[34].
111 The abnormalities of human and murine GATA1 hypomorphic MK include a content greater than
112 normal of TGF-β[35], CXCL1, the murine equivalent of IL-8[36], and P-SEL[37], three of the
113 proinflammatory proteins that have been implicated also in the development of IPF.

114 MK are important cellular components of the lungs where they exert the function to release
115 platelets (Plt) intravascularly[38,39] and to participate in immune reactions against opportunistic
116 infections[40,41]. In fact, by leveraging single cell RNA-seq and other methods, recent studies have

117 demonstrated the existence of three distinct types of MK, each one exerting a different function[41–
118 43]: The BM of adult mice and humans contains the Plt-producing, which correspond to the cells
119 previously defined as mature MK, and the niche-supportive and immune MK, both of which have
120 immature morphology. The Plt-producing MK are the most frequent, have high levels of ploidy,
121 express genes related to thrombopoiesis, including the transcription factor GATA1, and are
122 identified by the CD42b/ARNL markers. Niche-supportive MK are mostly >=8N and express high
123 levels of PF4 and TGF-β, and possibly of other pro- inflammatory cytokines, which regulate
124 growth of hematopoietic stem cells, and low levels of GATA1. These cells express the CD61 and
125 MYLK4 markers and may be induced in vitro by thrombopoietin to acquire a mature morphology
126 and to produce Plt. Immune-poised MK are low ploidy with signatures of inflammatory response
127 and myeloid leukocyte activation genes. These cells can be identified by the CD41 and LPS1
128 markers by confocal microscopy and by the CD41 and CD53 markers by flow cytometry. They
129 have phagocytic activity and can stimulate T cell expansion and have been identified in lungs
130 where their numbers increase in response to infectious challenges and are activated by neutrophil
131 netosis to phagocytize the infective agents[40,41]. Although previous studies had already implicated
132 MK abnormalities in the development of fibrosis in the lung of bleomycin-treated mice[44], the
133 pathobiological role of these cells in IPF is far from established. Based on the driving role exerted
134 by GATA1 hypomorphic MK in establishing fibrosis in the BM[30,31,34], we hypothesized that IPF
135 may be driven by a specific MK subpopulation with an abnormally low GATA1 content. Here, we
136 tested this hypothesis by comparing the MK subclasses and their GATA1 content in the lung from
137 patients with IPF and the non-diseased tissue of lung cancer patients and assessed whether lungs
138 from mice carrying the *Gata1*^{low} mutation contain abnormal MK and became fibrotic with age.

139

140 **Results**

141 ***The lung from patients with IPF contains an excess of GATA1 hypomorphic megakaryocytes***
142 ***biased for the immune lineage***

143 To determine the role of MK in the development of IPF, we first compared the frequency and
144 GATA1 content of MK (CD42b^{pos} cells) in lungs from IPF patients with those observed in the
145 non-diseased tissues of patients with lung cancer (three subject per group) by immunofluorescence
146 microscopy. The clinical features of the patients are described in **Table S1**. Hematoxylin-Eosin

147 and reticulin staining of consecutive sections confirmed the abnormal architecture and the presence
148 of fibrosis in the lung of IPF patients, but not in those from the no-IPF controls, validating the
149 diagnosis referred to us by the Anatomo-Pathology repository (Figure 1A, S1). MK were identified
150 with *similar* low frequency in lung sections from IPF and no-IPF subjects (5-10 vs 0.1-1 CD42b^{pos}
151 cells/Area, not statistically different). However, while most (80%) of the MK from the no-IPF
152 lungs contains robust levels of GATA1, GATA1 is detectable in less than 20% of the MK from
153 that of the IPF group (p<0.05) (**Figure 1A,B, S1**).

154 To assess whether reduced GATA1 content had affected the type of MK present in the lung of the
155 patients, confocal microscopy studies with markers specific for the three subpopulations were
156 performed (**Figure 1C,D**). MK with immune, HSC-supportive and Plt-poised phenotype were
157 recognized in the lungs from both no-IPF and IPF patients. However, the immune-subpopulation
158 was contained with a frequency significantly greater (by 2-fold) in lungs from IPF patients vs.
159 normal.

160 ***Megakaryocytes in the lungs from Gata1^{low} mice are immature and with age became biased for***
161 ***the immune-lineage and express a defective immune-signature***

162 To assess the effects of reduced GATA1 content on the MK present in the lung, we quantified the
163 frequency, maturation and lineage fate of MK present in mice harboring the *Gata1*^{low} mutation
164 (**Figure 2, S2**). MK (CD42b^{pos} cells) are readily identified in the lungs from both *Gata1*^{low} and
165 wild-type (WT) littermates (approximately 20 CD42b^{pos} cells/Areas) by both immune-
166 histochemistry and fluorescent analysis (**Figure 2A,B and S2A**). As expected only a minority
167 (<10%) of CD42b^{pos} cells from the lung of *Gata1^{low}* mice contains GATA1 while this transcription
168 factor is clearly detected in the vast majority (>90%) of those from the WT littermates (p<0.0001)
169 (**Figure 2B and S2B**).
170 The localization and maturation state of MK in lung sections from *Gata1^{low}* and their WT
171 littermates determined by morphological observations is compared in **Figures 2, S2C** and **Table**
172 **1**. MK are observed either intravascularly or within the perivascular interstitium in the lungs from
173 both WT and *Gata1*^{low} littermates (**Figure S3**). Most of the CD42b^{pos} megakaryoctes in the lungs
174 from WT mice have a mature morphology and are surrounded by structures resembling Plt (Plt
175 forming MK, PfMKs) (**Figure 2A, S2A, Table 1**). When detected in the alveolar septa, WT MK
176 are arranged in clusters (**Figure S2A**). By contrast, the MK in the lung from *Gata1*^{low} mice have

177 an immature morphology which includes a circular shape and scant cytoplasm (**Figure 2A, S2A,**
178 **Table 1**). We observed that a minority of the *Gata1*^{low} MK are surrounded by CD42b positive Plt
179 which would identify them as PfMKs (**Figure S2A)**. The few *Gata1*^{low} PfMKs are found isolated
180 near blood vessels inside the septa, have a reduced cytoplasm and an elongated nucleus that
181 extends itself between epithelial cells (**Figure S2A)**.

182 Statistical analyses of the frequency and maturation state of the MK observed in the lungs from a
183 large cohort of mice indicate that, without controlling for the effects of age or sex, the difference
184 in the frequency of total, immature and mature MK in the lung from WT and *Gata1*^{low} mice is
185 statistically significant (total $p=0.001$, immature $p<0.001$, mature $p=0.007$) (**Table 1**).

186 The maturation state of the MK in the lungs from WT and Gata1^{low} mice was further compared by
187 flow cytometry determinations of the ploidy state using the CD42b antibody coupled with
188 propidium iodide staining that assess the cell DNA content (Figure 2C*,* S2C). As expected[43]**,** the
189 ploidy of CD42b^{pos} cells in WT lungs ranged from 2N up to 64N with approximately 60% of the
190 cells displaying a DNA content >8N. This result confirms the morphological observation that most
191 of the ***MK*** present in WT lungs are mature. By contrast, the DNA content of the majority
192 (approximately ***80***%) of CD42b^{pos} cells from Gata1^{low} lungs is 4N and few (<20%) of them has a
193 DNA content greater than 8N, providing further indication that most of these cells are immature.

194 To assess whether reduced GATA1 content had affected the type of MK present in the lung of
195 *Gata1*^{low} mice, confocal microscopy studies with markers specific for the three MK subpopulations
196 were performed (**Figure 2D, S4**). These studies included WT mice as control and analyzed age as
197 independent variable. MK with HSC-supportive or Plt phenotype were recognized in the lungs
198 from both young and old WT and *Gata1*^{low} mice (**Figure 2D, S4**). The frequency of the two
199 populations was significantly greater than normal in the lungs from *Gata1*^{low} mice at both ages.
200 By contrast, immune-MK were not detected in the lungs from young and old WT mice and in
201 young *Gata1*^{low} mice but were present in robust numbers in those from old *Gata1*^{low} mice (**Figure**
202 **2E-G**).

203 To understand the effect of reduced GATA1 content on the expression profiling of the MK, we
204 performed RNAseq on purifed CD41^{+} cells (>95% CD41^{+} by re-analyses) from BM and lung of
205 15-months old WT and *Gata1*^{low} mice. Principal component analysis (PCA**)** of the RNAseq data
206 from individual mice indicate a strong separation and clustering among groups, with the

207 differences between tissue of provenience (BM or lung) accounting for approximately 79% of the
208 variance in the expression data (**Figure 2H and S5A**). Comparison of WT and *Gata1*^{low} cells
209 derived from the lung revealed extensive changes in gene expression (3,593 genes were up-
210 regulated and 1,837 genes were down-regulated) (**Figure 2I**). The expression of representative
211 genes characterizing the signatures of the three recently described Mk subpopulations[43] indicate
212 that the majority of the expression changes are found among immune-MK genes which are
213 downregulated (*Clec4a2*, *Il1b*, *Cxcl3*, *Cxcl5*, *Lcn2*, etc.) (**Figure 2J**). In addition, pathway analysis
214 indicated that pathways which regulate immune-functions (such as production of molecular
215 mediator of immune response, cell chemotaxis, activation of the immune-response, humoral
216 immune response, and immunoglobulin production) are among the top 10 pathways abnormally
217 expressed by *Gata1*^{low} MK (**Figure S5B,C**). Of note, MK purified from the BM and the lung of
218 *Gata1*^{low} mice displayed similar abnormalities, suggesting that they are driven by insufficient
219 expression of the transcription factor rather than by pro-inflammatory cytokines present in the lung
220 microenvironment (**Table S2**).

221 Collectively, these results demonstrate that the lungs from old *Gata1*^{low} mice contain increased
222 levels of immune-MK vs. normal and that the function of these cells is likely impaired.

223 ***Fibrosis is only present in Gata1*^{low} *mice***

224 The observation that the fibrosis in the lung from bleomycin-treated animal models is associated
225 with an inflammatory state induced by the chemical insult prompted us to detail the level of
226 inflammation and of fibrosis present in lungs from *Gata1*^{low} and WT littermates as they aged
227 (**Figure 3, Figures S3, S6, Table 1**).

228 Histological features consistent with interstitial pneumonia are observed in the lungs from a
229 significant number (>40%) of both the WT and *Gata1*^{low} mice analyzed (**Figures 3A** and **S3**).
230 More specifically, interstitial pneumonia (mild, moderate and severe) characterized by infiltration
231 of lymphocytes, macrophages and neutrophils in the alveolar septae and in the peri-bronchial-
232 vascular spaces, was observed in 9 out of 12 WT mice analyzed and in 27 out of 37 of the *Gata1*^{low}
233 mice (**Figure 3B**). In the *Gata1*^{low} mice, pneumonia extend from the alveolar septae to the
234 subpleural interstitium (**Figure S3**). Without controlling for the effects of age or sex, there are no
235 statistically significant differences in severity of lung inflammation between the two genotypes.
236 Sensitivity analyses adjusting for age and for sex also failed to find a statistically significant

237 difference (**Table 1**). Notably, the high level of inflammation observed in the lung of WT (CD1)
238 mice is consistent with previous studies on their baseline pathologies which showed they suffer
239 from acute inflammatory pathology, including pneumonia[45].

240 In contrast to the lack of inflammation differences, we found elevated incidence of fibrosis in lungs
241 from *Gata1*^{low} mice, but we observed it seldom in those from their WT littermates (**Figure 3A,**
242 **3C, S6, S7A**). Both by reticulin and Masson's tricrome staining, fibrosis is not detectable (66.7%)
243 or is overall mild (Grade 1, 33.3%) in the lungs from WT mice. By contrast, is absent only in a
244 minority (27.6%) of the lung from *Gata1*^{low} mice and is present at mild (Grade 1), moderate (Grade
245 2) or severe (Grade 3) levels in 31.03%, 27.59% and 13.79% of the mice in this group, respectively
246 (**Table 1**) with a penetrance of 85.71% at >22 months of age.

247 Without controlling for the effects of age or sex, there are statistically significant differences
248 between WT and *Gata1*^{low} mice in lung fibrosis as assessed by semiquantitative (p=0.01) or by
249 quantitative methods (p=0.006) (**Table 1**). In multivariable analysis, the formal test of interaction
250 between genotype and age was statistically significant (p=0.02); indicating that age is a statistically
251 significant modifier on the relationship between genotype and lung fibrosis. By contrast. there is
252 insufficient evidence to conclude there is a relationship between sex and fibrosis grade (p=0.99)
253 (**Figure 3E,F**). When stratifying by genotype, there is evidence of a statistically significant
254 relationship between age and lung fibrosis grade in *Gata1*^{low} mice (p<0.001), with lung fibrosis
255 grade increasing with increasing age; there is insufficient evidence to conclude there exists a
256 relationship between age and fibrosis grade in WT mice (p=0.26).

257 Taken together, these data suggest that mild interstitial pneumonia is to be considered a
258 background lesion of the CD1 strain, while fibrosis in the lungs is an age-associated trait in mice
259 harboring *Gata1*^{low} genetic lesions.

260 ***Lungs from old Gata1^{low} mice contain elevated levels of P-SEL, TGF-β1 and CXCL1 in cells***
261 ***with a megakaryocyte morphology***

262 Previous described results in mice indicated that in the bleomycin model, IPF is associated with
263 greater than normal expression of several pro-inflammatory factors including: P-selectin
264 (produced by endothelial cells); TGF-β (produced by several cell types including alveolar
265 macrophages, epithelial and endothelial cells, interstitial fibroblasts and Type II pneumocytes);
266 and CXCL1, the murine equivalent of human interleukin-8 (IL-8) in bronchoalveolar lavages[10,46–

267 [56]. Notably, some of these observations have been validated with samples from human fibrotic
268 patients [10,46–56].

269 We assessed whether the inflammatory milieu of the lungs from *Gata1*^{low} mice has similar
270 abnormalities by comparing the content of P-SEL, TGF-β1 and CXCL1 in the lungs from *Gata1*^{low}
271 and WT littermates by immunohistochemistry (**Figure 4**). Strikingly, we found that the lungs from
272 *Gata1*^{low} mice contain levels 10-fold greater than normal of P-SEL, 20-fold greater than normal of
273 TGF-β1 and 2-fold greater than normal of CXCL1 (**Figure 4A,B**). By morphological analysis, all
274 the pro-inflammatory proteins were expressed by endothelial cells, macrophages and neutrophils
275 also from lungs of *Gata1*^{low} mice and mutant type II pneumocytes contained levels greater than
276 those observed in WT cells of P-SEL and TGF-β1. In addition, cells with MK-like morphology
277 were readily detected only in lung sections immune-from *Gata1*^{low} mice stained for all the three
278 pro-inflammatory proteins. The high levels of TGF-β1 (fold-change 1.49, p=0.006) and P-sel (fold
279 change 1.63, p=0.031) contained in *Gata1*^{low} MK is consistent with the high expression of these
280 genes (**Table S2**).

281 We note that further support that the pro-inflammatory proteins produced by the abnormal MK
282 drive fibrosis in our model is provided by histo-morphological observations showing that MK
283 found in the lung of *Gata1*^{low} mice are embedded within the collagen fibers (**Figure S7**).

284 These results indicate that high expression of P-SEL, TGF-β1 and CXCL1 by endothelial cells,
285 bronchial epithelium and macrophages are drivers for lung inflammation observed in both WT and
286 *Gata1*^{low} littermates, but that expression of these pro-inflammatory proteins by type II
287 pneumocytes and MK are responsible for the increased bioavailability which leads to fibrosis in
288 the lungs of the mutant mice.

289 ***Fibrosis in the lung from Gata1^{low} mice is prevented by genetic ablation of P-selectin***

290 To assess the role of P-SEL in the pathogenesis of lung fibrosis, we compared the MK profile and
291 the histopathology of lungs from *Gata1*^{low} and from their *Gata1*^{low} littermates lacking *P-sel* with
292 age (**Figures 2A,3D-F, 5 *and* Tables 1** and **S2A**).

293 In the lung of mice carrying only the *P-sel*^{null} mutation, used as control, the total numbers of MK
294 were similar to those observed in WT littermates (**Table S3**). However, mature MK were less
295 frequent in lungs from *P-sel*^{null} mice than in those from WT littermates (**Figures 2A, S1** and **Table**

296 **S3).** Moreover, the lungs from *P-sel*^{null} mice manifest levels of inflammation not significantly
297 different from that expressed by WT mice (**Figure 5A, Table S3**). These results indicate that
298 deletion of *P-sel* has modest effects on the baseline inflammatory phenotype of the murine strain
299 used for this study. Critically, the WT littermates of *P-sel*^{null} mice did not develop fibrosis in the
300 lungs (**Figure 5A, 3D-F** and **Table S3**).

301 Although the lungs from *Gata1*^{low} and *P-sel*^{null}*Gata1*^{low} mice contain similar numbers of abnormal
302 MK (**Figure 2A,** and **Table 1**), the frequency of those expressing an immature phenotype was
303 greatly decreased in the lungs from the double mutants compared to the *Gata1*^{low} littermates. Also
304 in this case, the modestly higher rates of severe inflammation (grade 2 or 3) observed in *Gata1*^{low}
305 compared to *P-sel*^{null}*Gata1*^{low} mice (43.2% vs 27.8%) is not a statistically significant (unadjusted
306 p=0.27; age-adjusted p=0.08; sex-adjusted p=0.34) (**Figure 5A, Table 1**). However, lung fibrosis
307 is higher among *Gata1*^{low} compared to *P-sel*^{null}*Gata1*^{low} mice (Mean [±SD]=12. [±11.6] vs 5.2
308 [±5.3]). After adjusting for differences in sex or in age (age-adjusted p=0.04; sex-adjusted
309 p=0.002), the difference in lung fibrosis between the two group is statistically significant (**Figure
310 3D-F, Figure 5A, Table 1**).

311 Mechanistically, reduction of severe inflammation in mice lacking *P-sel* is associated with barely
312 detectable levels not only, as expected due to the genetic lesion, of P-SEL, but also of TGF-β and
313 CXCL1 (**Figure 4A,B**). As expected, single cell analyses indicate that genetic deletion of *P-sel*
314 reduced P-SEL content in endothelial cells, type II pneumocytes, bronchial epithelium,
315 macrophages but did not affect the content of TGF-β and CXCL1 in these cells with respect to WT
316 (compare **Figure S8 with Figure 4C**). By contrast, deletion of *P-sel* in *Gata1*^{low} mice specifically
317 reduced the content of TGF-β and CXCL1 in MK with respect to that observed in *Gata1*^{low} mice
318 (compare **Figure S8** with **Figure 4C**), providing support for the hypothesis that MK are the driver
319 for their increased microenvironmental bioavailability associated with lung fibrosis in *Gata1*^{low}
320 mice.

321 In conclusion, ablation of *P-sel* has modest effects on inflammation but, after adjusting for age and
322 sex, significantly reduces fibrosis in the lungs of *Gata1*^{low} mice. Reduction of fibrosis is associated
323 with reduced frequency of morphologically immature MK and of MK producing TGF-β1 and
324 CXCL1 in the lung.

325 ***Fibrosis in the lung from Gata1^{low} mice is rescued by inhibitors of P-selectin, TGF-β or CXCL1***

326 Given the role of pro-inflammatory factors involved in the development of lung fibrosis in
327 *Gata1*^{low} mice, we hypothesized that it may be to assess whether the pharmacologically reversible.
328 To test this, we treated, 12-month monthsold *Gata1*^{low} mice with the P-SEL neutralizing antibody
329 RB40.34, or the TGF-β1 trap AVID200 or the CXCR1/2, the receptor for CXCL1, inhibitor
330 Reparixin (**Figure 5B-D**). RB40.34 treatment significantly reduced not only inflammation but also
331 fibrosis in the lungs within 5 days. By day 40, 50% of the treated mice had no sign of lung
332 inflammation, and fibrosis was undetectableundetected by Masson staining and only persisted at
333 low level by reticulin staining. AVID200 treatment had modest effects on lung inflammation and
334 did not reduce fibrosis by reticulin staining, h. owever, it significantly decreased fibrosis detected
335 by Masson by 10 weeks **(Figure 5E-G**). CXCR1/2 inhibitor reduced, lung inflammation by day
336 20 and fibrosis was significantly reduced by reticulin staining both at day 20 and 37 and by Masson
337 at day 20 only (**Figure 5H-J)**.

338 Taken together, although inhibition of P-SEL, TGF-β1 or CXCL1 as single agents are all effective
339 in reverting fibrosis in the lungs from *Gata1*^{low} mice, a temporal gradient of efficacy was observed
340 among the three drugs with inhibition of P-SEL being the most effective. In fact, P-SEL inhibitors
341 were effective both at early and late points and reduced both reticulin and collagen fibers. TGF-β1
342 inhibitors were effective at late points only and reduced complex collagen deposition while
343 CXCR1/2 inhibitors were effective at early and late time points both on reticulin and collagen
344 fibers and at late time points on reticulin fibers only.

345 ***Inhibition of P-SEL reduces the content of both TGF-β1 and CXCL1 and increases that of***
346 ***GATA1 of the megakaryocytes***

347 Mechanistic insights on the effects exerted by the three pro-inflammatory inhibitors on the fibrosis
348 of the lung were obtained by investigating their effects on the TGF-β1, CXCL1 and GATA1
349 content of the MK (**Figure 6**). Treatment with the P-SEL inhibitor significantly reduced both the
350 TGF-β1 and CXCL1 content by day 5 and persisted up to day 40 **(Figure 6A-C)**. At the single cell
351 level, treatment with the P-SEL inhibitor reduced the TGF-β content in MK and that of CXCL1
352 both in MK and in type II pneumocytes (**Figure S9** and data not shown). Treatment with this
353 inhibitor also increased the GATA1 content of the MK (**Figure 6D,E**). By contrast, treatment with
354 either the TGF-β1 or the CXCR1/2 inhibitor significantly reduced only the CXCL1 content by the

355 end of the treatment without affecting that of TGF-β1 (**Figure 6A-C**). These reductions also were
356 more pronounced at the level of the MK (**Figure S9** and data not shown). The TGF-β1 and the
357 CXCR1/2 inhibitor did not significantly affect the GATA1 content of MK which remained low
358 **Figure 6F-I**). These results provide further support to the hypothesis that in *Gata1*^{low} mice IPF is
359 sustained by pro-inflammatory proteins, such as TGF-β1 and the CXCL1, produced by the
360 abnormal MK.

361

362 ## Discussion

363 We describe that the lungs of IPF patients and those from old mice harboring the *Gata1*^{low} mutation
364 which impairs expression of this gene in MK, contain MK expressing low levels of GATA1 and
365 biased toward the immune lineage. In addition, *Gata1*^{low} mice develop with age fibrosis in the
366 lung. These results suggest that abnormalities in the immune-MK populations produced by the BM
367 and sustained by low GATA1 content, represent possible drivers for IPF. Importantly, we propose
368 *Gata1*^{low} mice as a novel animal model for IPF.

369 Overall, the histological features of the fibrosis observed in the lung from *Gata1*^{low} mice are more
370 similar to that observed in IPF in patients than that displayed by the currently available bleomycin
371 model of the disease: i) as IPF patients, *Gata1*^{low} mice progressively develop both reticulin and
372 collagen fibrosis in the lungs as they age, recapitulating the chronic nature of the disease, while in
373 the bleomycin model fibrosis is an acute event retained until the insult persist. ii) although the lung
374 from *Gata1*^{low} mice never acquires the honeycomb morphology typical of those from IPF patients,
375 in the *Gata1*^{low} lung, as in those from the patients, fibrosis is present predominantly in the
376 subpleural region of the basal lobes and, occasionally, in the para-septal parenchyma while in
377 bleomycin-treated animals, fibrosis has a bronco centric localization that reflects the site where
378 the insult is applied; iii) as in IPF patients, inflammation is not the primary cause of fibrosis in the
379 lung from *Gata1*^{low} mice while fibrosis is a direct consequence of inflammation in bleomycin-
380 treated animals. The evidences that inflammation is not the primary driver of fibrosis in *Gata1*^{low}
381 mice are: i) inflammation is observed also in the lung from WT littermates which never develop
382 fibrosis; ii) genetic deletion of *P-sel* prevents development of fibrosis in the lung of mice carrying
383 the *Gata1*^{low} mutation but does not reduce the base-line inflammation of this organ; iii)
384 pharmacological inhibition of either P-SEL, TGF-β or CXCR1/2, has modest, if any, effect on

385 inflammation but rescues the fibrosis in the lung of *Gata1*^{low} mice. Based on these data, we
386 conclude that inflammation is a confounding factor rather than a cause of fibrosis in IPF and that
387 *Gata1*^{low} mice represent a model for IPF more stringent than the bleomycin-treated mice currently
388 used to study the etiology of this disease.

389 In the bleomycin-animal model, inflammation is initially associated with accumulation of
390 neutrophils within the lung, which are subsequently replaced by lymphocytes[57]. This accumulation
391 is associated with an increase in the levels of systemic and microenvironmental pro-inflammatory
392 cytokines (TGF-β, CXCL1 and others), which precede pro-fibrotic markers (fibronectin and pro-
393 collagen 1), eventually leading to fibrosis[5]. Abnormal expression of P-SEL by endothelial cells[10]
394 and of TGF-β by numerous cell types, including endothelial cells, epithelial cells, type II
395 pneumocytes and alveolar macrophages[50,51], has been implicated in the development of fibrosis in
396 the lungs of bleomycin-treated animals. In addition, although CXCL1 is elevated in bronco-
397 alveolar lavages of these mice[58], the cells responsible for its production are not yet been identified.
398 Some of these findings in mice have been validated by studies involving IPF patients[52,54,55,59 47–49]
399 but, by contrast with the results with the bleomycin mouse models, P-SEL is expressed at levels
400 greater than normal on the Plt from IPF patients[46]. However, since studies in the bleomycin model
401 are confounded by inflammation, it is not possible to discriminate the cells which produce factors
402 responsible for inflammation from those which produce factors responsible for fibrosis.

403 To address this, we used a combination of genetic and pharmacological approaches to dissect the
404 identity of the cells responsible to sustain these two pathological aspects in our model. By immune-
405 histochemistry analyses, endothelial and epithelial cells, alveolar macrophages and interstitial
406 fibroblasts from the lung not only of *Gata1*^{low} mice but also of their WT littermates and of *Psel*^{null}
407 mice, which express inflammation but no fibrosis, contain robust levels of P-SEL, TGF-β and/or
408 CXCL1, suggesting that the abnormal content of these proteins in these cells is responsible for the
409 baseline inflammation. By contrast, MK, and to some extent type II pneumocytes, are the cells that
410 contain robust levels of these pro-inflammatory mediators mainly in the lung from *Gata1*^{low} mice,
411 suggesting that these cells are responsible to establish the pro-inflammatory milieu that drives
412 fibrosis in this model. This interpretation is consistent with the observation that GATA1-deficient
413 immune MK are detectable in the lung from old *Gata1*^{low} mice and from IPF patients. In the case
414 of *Gata1*^{low} MK, their altered immune functions were confirmed by RNA-seq profiling which
415 includes upregulation of the inflammatory mediators TGF-β (fold-change= 1.49, p=0.006) and

416 CXCR2 the receptor for CXCL1[60,61] (fold change=1.95, p=0.007), and downregulation of factors
417 involved in the MK-specific anti-microbial response of the lung: *CXCL1* fold-change=2.8,
418 *p*=0.000), *CXCL5* (fold-change -2.691, *p*=0.017, and *CXCL10* (fold-change -1.88, *p*=0.033) [60–63].
419 The discrepancy between normal levels of *CXCL1* mRNA detected in the *Gata1*^{low} MK by RNA-
420 seq and their high *CXCL1* content detected by immunohistochemistry may be explained by the
421 high levels of the mRNA for *CXCL2*, a receptor which internalize its ligand without routing it to
422 the degradation system, expressed by these cells which allow accumulation of the protein in the
423 cell cytoplasm.

424 The pathogenetic role of P-SEL, TGF-β and CXCL1 in the fibrosis of the lung from *Gata1*^{low} mice
425 was further dissected by evaluating the effects of the deletion of *P-sel* and inhibition of P-SEL,
426 TGF-β and CXCR1/2 on the lung phenotype of these mice. Genetic deletion of *P-sel* prevented
427 the development of fibrosis in the lung from mice carrying the *Gata1*^{low} mutation with age. This
428 effect was associated with reduced content of both TGF-β and CXCL1 in the MK from this organ.
429 Furthermore, inhibition of P-SEL reduced fibrosis (both as reticulin and collagen fibers) quickly,
430 the effects were sustained upon the end of the treatment and were associated with significant
431 reductions in the frequency of MK with low GATA1 content and high TGF-β and CXCL1 content.
432 CXCR1/2 inhibition also reduced reticulin fibers both at early and late time points but reduced
433 collagen fibers only at early time points. The failure of Reparexin, the CXCL1/2 inhibitor tested
434 in our models to reduce collagen fibers at early time points is consistent with previous observations
435 indicating that this drug effectively reduces fibrosis in Bleomycin-treated mice which represent a
436 model for early stages of the disease[64,65]. The effects of the CXCR1/2 inhibitor were associated
437 with reduced CXCL1 content in the lung but the levels of TGF-β remained high and that of GATA1
438 remained low in the MK from the CXCR1/2 treated *Gata1*^{low} mice. Moreover, TGF-β inhibition
439 had modest effects on the reticulin fibers, reduced collagen fibers only at the latest time point and
440 the effects were associated with reduced CXCL1 content. As for CXCR1/2 inhibition, the TGF-β
441 content of the MK remained high and that of GATA1 remained low also upon TGF-β inhibition.
442 Although the effects exerted the TGF-β inhibitor on the fibrosis of the lung from *Gata1*^{low} mice
443 are inferior to those exerted by drugs inhibiting the same pathway in bleomycin-treated model,
444 they are consistent with the poor performance of drugs which inhibit a spectrum of pro-
445 inflammatory cytokines which include TGF-β clinically tested up to now in IPF[14–17].

446 Overall, these data suggest that in *Gata1*^{low} mice fibrosis in the lung is triggered by an abnormal
447 population of immune-MK which initiates a sequence of pathological effects exerted by multiple
448 pro-inflammatory proteins over time. The first step is accumulation of immune-MK and
449 engagement of these cells in a pathological cell interaction mediated by P-SEL. This cell
450 interaction increases the bioavailability of TGF-β and CXCL1, and possibly of other
451 proinflammatory cytokines not identified as yet, in the microenvironment that sustain the cell
452 mesenchymal transition responsible for fibrosis. The cell undergoing the mesenchymal transition
453 in the *Gata1*^{low} lung has not been identified as yet. However, since the genes encoding the
454 extramedullary matrix are down-regulated in the RNA-seq profiling of the *Gata1*^{low} MK from the
455 lung (**Figures S5C** and **S7**), we exclude that this population is represented by the niche-poised
456 MK, a population responsible to synthesize the extracellular matrix during organo-genesis[42] and
457 that, when pathologically reactivated in adulthood, promote scarring of the BM[25].

458 The finding that *Gata1*^{low} mice develop with age both myelofibrosis and fibrosis in the lung is
459 counterintuitive with respect to the clinical practice. In fact, patients with MF, a disease driven by
460 mutations in the hematopoietic stem cells which reduces GATA1 content in MK, include
461 development of pulmonary hypertension[66] but not of lung fibrosis (Dr. Hoffman, personal
462 communication) while those with IPF seldom develop myeloproliferative neoplasms (Dr. Richeldi,
463 unpublished observations). This apparent paradox is reconciliated by the observation that in
464 *Gata1*^{low} mice myelofibrosis and IPF are driven by two distinctive MK populations: Myelofibrosis
465 is sustained by reactivation of the differentiation of the niche-MK, a population which plays an
466 important role during organogenesis which is absent in adult BM[42] and that is responsible to
467 produce collagen in the BM on these patients[25]. By contrast, our data indicate that in IPF, fibrosis
468 is driven by pro-inflammatory proteins produced by the abnormal immune-MK. In other words,
469 the mutations (or epigenetic events) that drive myelofibrosis and those, still to be identified, that
470 drive IPF sustain the generation of abnormal GATA1^{low} MK belonging to different lineages:
471 GATA1^{low} niche-supporting MK are responsible for myelofibrosis and GATA1^{low} immune-MK
472 for IPF. Since the *Gata1*^{low} mutation affects the GATA1 content of MK of all lineages, it mimics
473 downstream effects induced by both the myelofibrosis and IPF driver mutations and the *Gata1*^{low}
474 mice develop both phenotypes. Indirect support for this hypothesis, is provided by the observation
475 that loss of telomerase function predisposes not only to IPF but also to aplastic anemia[19], a
476 condition associated with hematopoietic failure and insufficient production of MK[67]. We

477 hypothesize that the epigenetic reprogramming (or genetic event) restricting the differentiation
478 potential of hematopoietic stem cells toward the MK lineage occurring during the process of clonal
479 hematopoiesis associated with aging [68], determines whether telomerase-deficient hematopoietic
480 stem cells will generate GATA1^{low} immune-MK, resulting in IPF. In this regard, cells of BM origin
481 had been already associated with development of IPF[69], leading to the interesting therapeutic
482 hypothesis that IPF may be treated with BM transplantation[70].

483 In conclusion, *Gata1^{low}* mice are the first genetically driven IPF animal model and provide strong
484 evidence that immune-MK alterations play a major role in the development of this disease. The
485 *Gata1*^{low} model also clarifies that P-SEL dysregulation predates TGF-β and CXCL1 in the
486 pathobiology of IPF and should be considered for treatment of these patients.

487

488 **Limitations of study**

489 The limitations of this study are: 1) insufficient evidence that the molecular abnormalities of the
490 immune MK found in the lungs from IPF patients are similar to that found in the cells from
491 *Gata1^{low}* mice; 2) insufficient evidence that the *Gata1^{low}* mutation drives the IPF phenotype in a
492 cell autonomous fashion and 3) insufficient evidence in support of innovative therapeutic options
493 in IPF. Limitation 1) will be addressed by additional studies investigating the abnormalities of the
494 MK and the hematopoietic stem cells from IPF patients. Limitation (2) will be addressed by
495 demonstrating that WT mice develop fibrosis in the lungs when transplanted with *Gata1*^{low}
496 hematopoietic stem cells while the fibrosis in the lungs of *Gata1*^{low} mice is cured by transplantation
497 with WT hematopoietic stem cells. The experiments, that will be done as part of separate studies,
498 required to overcome limitation 1 and 2 will also overcome limitation (3) by providing preclinical
499 rational to test the beneficial effects of BM transplantation for IPF.

500 **Acknowledgments**

501 This study was supported by grants from the National Cancer (P01-CA108671 ARM) and
502 Associazione Italiana Ricerca Cancro (AIRC IG23525, ARM). Profs. Antonia D'Errico, Ilaria
503 Bassi and Simone Carotti are gratefully acknowledged for providing access to the tissue repository
504 of St. Orsola Hospital, Bologna and Campus Bio-medico, Rome, Italy.

505 **Author contributions**

506 FG, MZ, PV, MF, FA, FM and GS performed experiments and analyzed data. MM and JV
507 performed the RNA-seq analysis. CMH and ACD did the statistical analysis. AP, GS, SN, and LR
508 reviewed the data and wrote the manuscript. ARM, designed the experiments, analyzed and
509 reviewed the data and wrote the manuscript. All the authors read the manuscript, concur with its
510 content and approved the submission.

511 **Declaration of Interest**

512 The authors declare that the research was conducted in the absence of any commercial or financial
513 relationships that could be construed as a potential conflict of interest. ARM received funding for
514 research from Dompé Pharmaceutics, Forbius, Novartis for other projects.

515 **Methods**

516 ***Human Subjects***. Consecutive lung sections from IPF and non-IPF patients (three different
517 patients per group) were provided, respectively, by the Institute of Human Pathology, Policlinico
518 Sant'Orsola, Bologna, Italy and by Policlinico Campus Bio-Medico (Rome). Details of the
519 subjects included in the study are provided in **Table S1**. This is not a human study because all the
520 human specimens were provided as de-identified material by public repositories and it is not
521 subjected to prior IRB approval according to the Declaration of Helsinki for Studies Involving
522 Human Subjects.

523 ***Mice***. Male and female WT, *P-sel*^{null}, *Gata1*^{low} and *P-sel*^{null}*Gata1*^{low} mice were generated in the
524 animal facility of Istituto Superiore di Sanità as previously described [71]. All the mutations are in
525 the CD1 background. The study was approved by the Italian Ministry of Health (protocol n.
526 419/2015-PR and D9997.121) and conducted according to the European Directive 2010/63/EU for
527 the protection of animals used for scientific purposes.

528 ***Treatments.*** *P-SEL inhibitors:* Twenty 8-11 months-old *Gata1*^{low} mice were randomly divided in
529 two groups which were treated either with vehicle (2% v/v dimethyl sulfoxide in H_2O) or with
530 biotinylated mAb RB40.34 (BD Pharmigen, San Diego, CA; 30 µg/mouse every other day by tail
531 vein injection), as described [72,73]. Mice were sacrificed after 5-12-40 days for histopathologic
532 determinations. *TGF-β1 inhibitors*: *Gata1*^{low} mice (10 - 12 months-old) were weighted and

533 randomly divided into two groups (four males and four females/group) and treated with either
534 vehicle (PBS) or with the TGF-β1 trap AVID200 (5mg/Kg twice a week by intraperitoneal
535 injection), as described[74]. Mice were treated either for 42 (six mice, three females and three males
536 with AVID200 and 2 females with vehicle) or 72-78 (eight mice, four females and four males in
537 each group) days. At day 42, 72 or 78 from the beginning of the treatment, mice were euthanized,
538 and their lung removed for histopathology observations. *CXCR1/CXCR2 inhibitors*: Sixteen eight-
539 month-old *Gata1*^{low} mice were anesthetized with 2-to-3% isoflurane and implanted
540 subcutaneously with an ALZET® Osmotic Pump (model 2002) pre-filled with 200µL of vehicle
541 (sterile saline) or the CXCR1/CXCR2 inhibitor Reparixin (7.5mg/h/Kg in sterile saline) as
542 described [75,76]. Mice were sacrificed after 17 or 37 days after treatment, and their lungs removed
543 for histopathological determinations.

544 ***Histochemistry***. Lung and bone marrow (BM) from WT, *Gata1*^{low}, *P-sel*^{null} and *P-sel*^{null}*Gata1*^{low}
545 mice were fixed in 10% (vol/vol) phosphate-buffered formalin, paraffin embedded and cut into
546 consecutive 3µm sections, according to standard procedures. Consecutive sections from the mouse
547 organs, as well as from BM and lungs of the patients, were stained with Hematoxylin-Eosin (H&E,
548 cat no. 01HEMH2500 and 01EOY101000, respectively; Histo-Line Laboratories, Milan, Italy),
549 Reticulin (Bio-Optica, Milan, Italy) or Masson's trichrome (Bio-Optica) and evaluated with a
550 Nikon Eclipse E600 microscope (Nikon Instruments Europe BV, Amsterdam, NL) equipped with
551 the Imaging Source "33" Series USB 3.0 Camera (DFK 33UX264; Bremen, DE). Inflammation
552 was assessed on de-identified H&E stained sections by an experienced veterinarian pathologist
553 and expressed on the basis of a semiquantitative scale based on the numbers of inflammatory cells
554 (neutrophils, macrophages and lymphocytes) that were infiltrating the alveolar septae and/or
555 peribronchial-vascular spaces: grade 0 (absence of inflammatory cells); grade 1 (rare inflammatory
556 cells in <10% of the area); grade 2 (moderate numbers of inflammatory cells in 10-30% of the
557 area) and grade 3 (presence of large numbers inflammatory cells in >30% of the area). Fibrosis.
558 Semiquantitative and quantitative assessment of fibrosis were performed on sections stained with
559 Reticulin or Masson's trichrome staining by an experienced veterinary pathologist and by Image
560 analysis using the software ImageJ (version 1.52t, National Institutes of Health, Bethesda, MD,
561 USA), respectively. The semiquantitative scoring was the following: grade 0 (presence of collagen
562 fibers only at the bronchovascular level and absence of septal alveolar fibrosis); grade 1 (presence
563 of focal mature collagen fibers in the alveolar-septal interstitium); grade 2 (deposition of multifocal

564 to coalescing collagen fibers in the alveolar-septa interstitium); grade 3 (deposition of collagen
565 bundles that irregularly thicken the alveolar septa and alterations of the overall pulmonary
566 architecture) (**Figure S4A**). Quantitative image analysis was performed on five different
567 photomicrographs randomly selected per each lung section/mouse (area of each
568 photomicrograph=1.49mm^2) (**Figure S4B**). The number of mice analysed per experimental group
569 is indicated in the legends. Fibrosis was expressed as percent of the area stained in blue with respect
570 to the total area of the field censored of the empty alveolar spaces. Statistical analyses confirmed
571 a good correlation between the semiquantitative and quantitative determinations of fibrosis
572 (**Figure S4C**).

573 ***Immunofluorescence (IF) studies.*** Mouse and human lung and sections (3µm thick each) were
574 dewaxed in xylene and treated with EDTA (buffer pH=8), incubated for 20min in a pressure cooker
575 (110-120°C, high pressure) for antigen retrieval and then with antibodies against CD42b (cat no.
576 ab183345, Abcam, Cambridge, UK) or/and GATA1 (cat no. sc-265, Santa Cruz Biotechnology,
577 Santa Cruz, CA, USA), Collagen I (cat no. NB600-408, Novus biologicals, Centennial, CO, USA),
578 Collagen III (cat no. ab7778, Abcam) or Collagen IV (cat no. ab6586, Abcam) over night at 4°C.
579 Cell binding of the primary antibodies was visualized with a secondary antibody goat anti-rat
580 Alexa Fluor 488 (cat no. ab150165, Abcam) or anti-rabbit Alexa Fluor 555 (cat no. ab150078,
581 Abcam), as appropriate. Sections were counterstain with DAPI (cat no. D9542-5MG, Sigma
582 Aldrich, Saint Louis, MI, USA) and mounted with Fluor-shield histology mounting medium (cat
583 no. F6182-10MG, Sigma Aldrich). The slides were examined using a Nikon Eclipse Ni microscope
584 equipped with the appropriate filter cubes to distinguish the fluorochromes employed. The images
585 were recorded with a Nikon DS-Qi1Nc digital camera and NIS Elements software BR 4.20.01 and
586 selected sections were acquired using FV1000 confocal microscope (Olympus, Tokyo, Japan)
587 equipped with a confocal spectral imaging system (Olympus Fluoview 1000). The number of
588 megakaryocytes was counted in 10 fields per section and expressed as mean value.

589 ***Confocal Microscopy.*** Femurs were fixed in formaldehyde (10% v/v with neutral buffer), treated
590 for 1h with a decalcifying kit (Osteodec; Bio-Optica, Milan, Italy) and included in paraffin. Three
591 micron-thick BM sections were dewaxed in xylene and antigens were retrieved by treatment with
592 EDTA buffer (pH=8) for 20' in a pressure cooker (110-120°C, high pressure). For each sample
593 almost 3 consecutive sections were obtained. One was incubated with antibodies against CD41
594 (rat anti mouse, Santacruz Biotechnology INC. (MWReg30): sc-19963) and LSP1 ([EPR5997].

595 Another one with monoclonal rabbit anti mouse (Abcam cat. ab133506) and the last one incubated
596 with antibodies against CD61 ((B-7) mouse anti mouse, Santacruz Biotechnology INC., sc-46655)
597 conjugated with Alexa 488, and MYLK (polyclonal rabbit anti-mouse, Proteintech, 24309-1-AP);
598 and the last one incubated with antibodies against CD42b (mouse monoclonal, Santacruz
599 Biotechnology INC, sc-271171) and ARNTL (rabbit anti mouse/human NB100-2288, Bio-
600 Techne), for 2 hours at room temperature. After extensive washing, sections were incubated for
601 45 min at room temperature with the following secondary antybody: CD41 was visualized with
602 the antibody goat anti rat Alexa Fluor 488 (Catalog #A-11006, Invitrogen); the LSP1, CD42b and
603 MYLK antibodies were visualized with the antibody donkey anti-rabbit Alexa Fluor 555 (Catalog
604 # A-31572, Invitrogen) and ARNTL was visualized with the antibody goat anti mouse Alexa Fluor
605 488 (Catalog #A32723, Invitrogen), CD61 is directly conjugated with Alexa 488. All sections were
606 mounted with Mounting Medium With DAPI - Aqueous, Fluoroshield (Catalog #ab104139,
607 Abcam) and examined using a confocal microscope Zeiss LSM 900 (Carl Zeiss GmbH, Jena,
608 Germany) in Airyscan mode, using a (Zeiss) planapo objective 60x oil A.N. 1,42. Excitation light
609 was obtained by a Laser Dapi 408 nm (DAPI), an Argon Ion Laser (488 nm) for Alexa 488 and a
610 Diode Laser HeNe (561 nm) for Alexa 555. DAPI emission was recorded from 415 to 485 nm,
611 Alexa 488 emission was recorded from 495 to 550 nm, Alexa 555 emission was recorded from
612 583 to 628 nm. Images recorded have an optical thickness of 0.3 μm and were processed with the
613 Zen Blue (3.2) (Carl Zeiss GmbH, Jena,Germany) and ImageJ (1.53t – National Institutes of
614 Health, USA, http://imagej.nih.gov/ij) softwares. All images were collected with the same detector
615 value for DAPI, Alexa 488 and Alexa 555, respectively. The background of each signal was
616 calculated splitting the channels and the single channel background obtained in areas external to
617 cells. The number of positive cells were obtained in the whole section(s).

618 ***Immunohistochemistry (IHC).*** Three micron-thick lung sections were dewaxed and rehydrated.
619 Endogenous peroxidase was blocked by immersion in H_2O_2 in methanol (3%, v/v) for 30' at room
620 temperature. Antigen retrieval was performed by incubation in citrate buffer, pH=6.0 for 1min in
621 a microwave oven at 750W, followed by cooling at room temperature for 20'. After blocking of
622 non-specific antigenic sites by incubation with goat serum in PBS (10%, v/V) for 30' at room
623 temperature, slides were incubated with CD42b (cat no. ab183345, Abcam, Cambridge, UK),
624 biotinylated anti-P-SEL (cat no. 553743, BD Pharmigen), anti-TGF-β1 (cat no. sc-130348, Santa
625 Cruz Biotechnology), anti-CXCL1 (cat no. ab86436, Abcam), anti-CXCR1 (cat no. GTX100389,

626 Genetex, Irvine, CA, USA) and anti-CXCR2 (cat no. ab14935, Abcam) antibodies overnight at
627 4°C. Binding sites were revealed with the commercial avidin-biotin-peroxidase kit (ABC Kit Elite,
628 Vector, Burlingame, CA) and the chromogen 3,3′-diaminobenzidine (0.05%, Histo-Line
629 Laboratories) either directly or previous incubation with suited secondary biotinylated antibodies.
630 Slides were counterstained with Harris hematoxylin (Histo-Line Laboratories) and mounted with
631 HistoMount DPX medium (cat no. 01BM500H, Histo-Line Laboratories). Image analysis was
632 performed using ImageJ program and the content of antibody binding was calculated as intensity
633 of the brown staining above the threshold in areas (1.49mm^2 each) from 5 different
634 photomicrographs randomly selected for each sample. The intensity of the staining of individual
635 cells recognized according to standard morphological criteria was arbitrarily assessed as "–"
636 (below detection), "+" (detectable) and "++" (strongly detectable).

637 ***Flow cytometry of lung megakaryocytes.*** Lungs were incubated in Dulbecco's modified Eagle
638 Medium (cat no. D8537, Sigma-Aldrich, Saint Lois, M0, USA), supplemented with 10% (v/v)
639 fetal bovine serum (cat no. F7524, Signa Aldrich), penicillin/streptomycin (cat. no. 15140122),
640 vitamins (cat no. 11120052), Glutamax (cat. no. 10566016), non-essential amino acids (cat no.
641 11140050) and sodium pyruvate (cat no. 11360070) plus collagenase type II (1mg/mL, cat no.
642 17101015) (all from Gibco; Grand Island, NY, USA), as described[43]. After 30min at 37°C, lungs
643 were mashed through a 100-µm cell strainer (BD Pharmingen) and washed with cold media and
644 centrifuged at 1200 rpm for 5 minutes. ACK Lysing Buffer (cat no. A1049201, Gibco) was added
645 to the pellet for 5 minutes in ice. The ACK was washed out with 50 mL of PBS and centrifuged at
646 1200 rpm for 5min. Cells were then incubated with phycoerythrin (PE)-CD41 (cat no. 558040)
647 and fluorescein isothiocyanate (FITC)-CD61 (cat. no. 553346). Dead cells were excluded by Sytox
648 Blue staining (0.002mM, Molecular Probes, Eugene, OR, USA). For DNA content determinations,
649 cells were then incubated with phycoerythrin (PE)-CD42b (cat. no. 555473) and FITC-CD61,
650 washed and fixed with 4% paraformaldehyde (Sigma-Aldrich) for 60min, permeabilized with
651 Triton-X100 (0.2% v/v in PBS, cat. no. 108643; Merck, Darmstadt, Germany) for 15min and
652 incubated with propidium iodide (40 µg/mL in PBS) and RNase A (100units/mL, cat. no.
653 10109142001, Merck) for 30min at 37°C. All the antibodies are from BD Pharmingen. Cells were
654 analyzed with Gallios (Beckman Coulter, Brea, CA, USA) and the flow cytometry data processed
655 with the Kaluza program (version 2.1, Beckman Coulter).

656 ***RNA seq analysis.*** MK were purified from the BM and lungs of two *Gata1*^{low} and three WT
657 littermates (11-25 months of age. Total RNA was collected using the Direct-zol™ RNA MiniPrep
658 (>200,000 sorted Megakaryocytes) or MicroPrep (<200,000 sorted Megakaryocytes) (Zymo
659 Reaserch). Illumina libraries were constructed using SMARTer Stranded Total RNA-Seq Kit v3 -
660 Pico Input Mammalian (TaKaRa, Japan). RNA-seq libraries were sequenced at read lengths 2 x
661 151bp on the Illumina Novaseq 6000 (Illumina). Aligment was performed using RNA-STAR
662 (2.3.1) using the ENCODE 4 default transcriptome annotation (GENCODE v25). Gene counts
663 were obtained using featureCounts and FPKM per gene were calculated using Cufflinks.
664 Differentially expressed genes (DEGs) between the two groups of lungs megakaryocytes from
665 *Gata1*^{low} mice and WT mice were analyzed with R package DESeq2 and the GO Enrichment
666 Analysis was performed with R package enrichplot, DOSE[77] and clusterProfiler [78,79]. Multiple
667 testing correction was performed using the Benjamini-Hochberg method and significance was
668 established at an FDR of 5%.

669 ***Gene Set Enrichment Analysis.*** GSEA was performed using GSEA software GSEA 4.3.1 wiTH
670 default parameters. The CURATED gene set (m2.all.v2022.1.Mm.symbols.gmt) used for the
671 analysis was downloaded from MSigDB
672 (https://www.broadinstitute.org/gsea/msigdb/collections.jsp). A total of 32,527 expressed genes
673 were included in the analysis. Genes were pre-ranked in order of their differential expression
674 between megakaryocytes from *Gata1*^{low} lungs and from CD1 lungs.

675 ***Statistical methods.*** Categorical variables are presented as counts and percentages by genotype;
676 Fisher's exact tests were used to test the univariate association between genotype and outcome.
677 Continuous variables are presented as mean (standard deviation [SD]), median, and range).
678 Statistical analyses was performed by parametric t-test or one-way ANOVA for multiple
679 comparisons, as appropriate. Multiple linear regression and ordinal logistic regression were used
680 to model relationships between genotype and outcomes, adjusted by age or by sex. Multiple linear
681 regression was used to test the interaction between age and genotype on the outcome of percent
682 fibrosis. Where interaction was found, simple linear regression was used to assess the relationships
683 between fibrosis outcomes and age, stratified by genotype. Alignment between semiquantitative
684 and quantitative levels of fibrosis was assessed using box plots. All hypothesis testing was two-
685 sided, with $p<0.05$ used as the threshold for statistical significance. Analyses were conducted using

686 SAS software (version 9.4; SAS Institute Inc., Cary, NC, USA), R (version 3.6.3), and Prism 8
687 (version 8.0.2; GraphPad Software, La Jolla, CA).

688 **References**

689 (1) Lederer, D. J.; Martinez, F. J. Idiopathic Pulmonary Fibrosis. *N Engl J Med* **2018**, *378* (19),
690 1811–1823. https://doi.org/10.1056/NEJMra1705751.

691 (2) Martinez, F. J.; Collard, H. R.; Pardo, A.; Raghu, G.; Richeldi, L.; Selman, M.; Swigris, J.
692 J.; Taniguchi, H.; Wells, A. U. Idiopathic Pulmonary Fibrosis. *Nat Rev Dis Primers* **2017**,
693 *3* (1), 17074. https://doi.org/10.1038/nrdp.2017.74.

694 (3) Richeldi, L.; Collard, H. R.; Jones, M. G. Idiopathic Pulmonary Fibrosis. *The Lancet*.
695 England 2017, pp 1941–1952. https://doi.org/10.1016/S0140-6736(17)30866-8.

696 (4) Mekhael, O.; Naiel, S.; Vierhout, M.; Hayat, A. I.; Revill, S. D.; Abed, S.; Inman, M. D.;
697 Kolb, M. R. J.; Ask, K. Mouse Models of Lung Fibrosis. *Methods Mol Biol* **2021**, *2299*,
698 291–321. https://doi.org/10.1007/978-1-0716-1382-5_21.

699 (5) Hay, J.; Shahzeidi, S.; Laurent, G. Mechanisms of Bleomycin-Induced Lung Damage. *Arch*
700 *Toxicol* **1991**, *65* (2), 81–94. https://doi.org/10.1007/BF02034932.

701 (6) Borzone, G.; Moreno, R.; Urrea, R.; Meneses, M.; Oyarzún, M.; Lisboa, C. Bleomycin-
702 Induced Chronic Lung Damage Does Not Resemble Human Idiopathic Pulmonary Fibrosis.
703 *Am J Respir Crit Care Med* **2001**, *163* (7), 1648–1653.
704 https://doi.org/10.1164/ajrccm.163.7.2006132.

705 (7) Nicholson, A. G.; Fulford, L. G.; Colby, T. V; du Bois, R. M.; Hansell, D. M.; Wells, A. U.
706 The Relationship between Individual Histologic Features and Disease Progression in
707 Idiopathic Pulmonary Fibrosis. *Am J Respir Crit Care Med* **2002**, *166* (2), 173–177.
708 https://doi.org/10.1164/rccm.2109039.

709 (8) Fernandez, I. E.; Eickelberg, O. The Impact of TGF-β on Lung Fibrosis. *Proc Am Thorac*
710 *Soc* **2012**, *9* (3), 111–116. https://doi.org/10.1513/pats.201203-023AW.

711 (9) Yang, L.; Herrera, J.; Gilbertsen, A.; Xia, H.; Smith, K.; Benyumov, A.; Bitterman, P. B.;
712 Henke, C. A. IL-8 Mediates Idiopathic Pulmonary Fibrosis Mesenchymal Progenitor Cell
713 Fibrogenicity. *American Journal of Physiology-Lung Cellular and Molecular Physiology*
714 **2018**, *314* (1), L127–L136. https://doi.org/10.1152/ajplung.00200.2017.

715 (10) Serrano-Mollar, A. P-Selectin Upregulation in Bleomycin Induced Lung Injury in Rats:
716 Effect of N-Acetyl-L-Cysteine. *Thorax* **2002**, *57* (7), 629–634.
717 https://doi.org/10.1136/thorax.57.7.629.

718 (11) Huang, C.-Y.; Chung, C.-L.; Hu, T.-H.; Chen, J.-J.; Liu, P.-F.; Chen, C.-L. Recent Progress
719 in TGF-β Inhibitors for Cancer Therapy. *Biomedicine & Pharmacotherapy* **2021**, *134*,
720 111046. https://doi.org/10.1016/j.biopha.2020.111046.

721 (12) Sime, P. J.; Xing, Z.; Graham, F. L.; Csaky, K. G.; Gauldie, J. Adenovector-Mediated Gene
722 Transfer of Active Transforming Growth Factor-Beta1 Induces Prolonged Severe Fibrosis
723 in Rat Lung. *Journal of Clinical Investigation* **1997**, *100* (4), 768–776.
724 https://doi.org/10.1172/JCI119590.

725 (13) Liu, J.-Y.; Sime, P. J.; Wu, T.; Warshamana, G. S.; Pociask, D.; Tsai, S.-Y.; Brody, A. R.
726 Transforming Growth Factor- β_1 Overexpression in Tumor Necrosis Factor- α Receptor
727 Knockout Mice Induces Fibroproliferative Lung Disease. *Am J Respir Cell Mol Biol* **2001**,
728 *25* (1), 3–7. https://doi.org/10.1165/ajrcmb.25.1.4481.

729 (14) Noble, P. W.; Albera, C.; Bradford, W. Z.; Costabel, U.; Glassberg, M. K.; Kardatzke, D.;
730 King, T. E. J.; Lancaster, L.; Sahn, S. A.; Szwarcberg, J.; Valeyre, D.; du Bois, R. M.
731 Pirfenidone in Patients with Idiopathic Pulmonary Fibrosis (CAPACITY):
732 Two Randomised Trials. *Lancet* **2011**, *377* (9779), 1760–1769.
733 https://doi.org/10.1016/S0140-6736(11)60405-4.

734 (15) King, T. E. J.; Bradford, W. Z.; Castro-Bernardini, S.; Fagan, E. A.; Glaspole, I.; Glassberg,
735 M. K.; Gorina, E.; Hopkins, P. M.; Kardatzke, D.; Lancaster, L.; Lederer, D. J.; Nathan, S.
736 D.; Pereira, C. A.; Sahn, S. A.; Sussman, R.; Swigris, J. J.; Noble, P. W. A Phase 3 Trial of
737 Pirfenidone in Patients with Idiopathic Pulmonary Fibrosis. *N Engl J Med* **2014**, *370* (22),
738 2083–2092. https://doi.org/10.1056/NEJMoa1402582.

739 (16) Richeldi, L.; Cottin, V.; Flaherty, K. R.; Kolb, M.; Inoue, Y.; Raghu, G.; Taniguchi, H.;
740 Hansell, D. M.; Nicholson, A. G.; Le Maulf, F.; Stowasser, S.; Collard, H. R. Design of the
741 INPULSIS™ Trials: Two Phase 3 Trials of Nintedanib in Patients with Idiopathic
742 Pulmonary Fibrosis. *Respir Med* **2014**, *108* (7), 1023–1030.
743 https://doi.org/10.1016/j.rmed.2014.04.011.

744 (17) Cerri, S.; Monari, M.; Guerrieri, A.; Donatelli, P.; Bassi, I.; Garuti, M.; Luppi, F.; Betti, S.;
745 Bandelli, G.; Carpano, M.; Bacchi Reggiani, M. L.; Tonelli, R.; Clini, E.; Nava, S. Real-
746 Life Comparison of Pirfenidone and Nintedanib in Patients with Idiopathic Pulmonary
747 Fibrosis: A 24-Month Assessment. *Respir Med* **2019**, *159*, 105803.
748 https://doi.org/10.1016/j.rmed.2019.105803.

749 (18) Hunninghake, G. M.; Quesada-Arias, L. D.; Carmichael, N. E.; Martinez Manzano, J. M.;
750 Poli De Frías, S.; Baumgartner, M. A.; DiGianni, L.; Gampala-Sagar, S. N.; Leone, D. A.;
751 Gulati, S.; El-Chemaly, S.; Goldberg, H. J.; Putman, R. K.; Hatabu, H.; Raby, B. A.; Rosas,
752 I. O. Interstitial Lung Disease in Relatives of Patients with Pulmonary Fibrosis. *Am J Respir*
753 *Crit Care Med* **2020**, *201* (10), 1240–1248. https://doi.org/10.1164/rccm.201908-1571OC.

754 (19) Arias-Salgado, E. G.; Galvez, E.; Planas-Cerezales, L.; Pintado-Berninches, L.; Vallespin,
755 E.; Martinez, P.; Carrillo, J.; Iarriccio, L.; Ruiz-Llobet, A.; Catalá, A.; Badell-Serra, I.;
756 Gonzalez-Granado, L. I.; Martín-Nalda, A.; Martínez-Gallo, M.; Galera-Miñarro, A.;
757 Rodríguez-Vigil, C.; Bastos-Oreiro, M.; Perez de Nanclares, G.; Leiro-Fernández, V.; Uria,
758 M.-L.; Diaz-Heredia, C.; Valenzuela, C.; Martín, S.; López-Muñiz, B.; Lapunzina, P.;
759 Sevilla, J.; Molina-Molina, M.; Perona, R.; Sastre, L. Genetic Analyses of Aplastic Anemia
760 and Idiopathic Pulmonary Fibrosis Patients with Short Telomeres, Possible Implication of
761 DNA-Repair Genes. *Orphanet J Rare Dis* **2019**, *14* (1), 82. https://doi.org/10.1186/s13023-
762 019-1046-0.

763 (20) Gable, D. L.; Gaysinskaya, V.; Atik, C. C.; Talbot, C. C. J.; Kang, B.; Stanley, S. E.; Pugh,
764 E. W.; Amat-Codina, N.; Schenk, K. M.; Arcasoy, M. O.; Brayton, C.; Florea, L.; Armanios,
765 M. ZCCHC8, the Nuclear Exosome Targeting Component, Is Mutated in Familial
766 Pulmonary Fibrosis and Is Required for Telomerase RNA Maturation. *Genes Dev* **2019**, *33*
767 (19–20), 1381–1396. https://doi.org/10.1101/gad.326785.119.

768 (21) Armanios, M. Telomerase and Idiopathic Pulmonary Fibrosis. *Mutation*
769 *Research/Fundamental and Molecular Mechanisms of Mutagenesis* **2012**, *730* (1–2), 52–
770 58. https://doi.org/10.1016/j.mrfmmm.2011.10.013.

771 (22) Zhang, K.; Wang, L.; Hong, X.; Chen, H.; Shi, Y.; Liu, Y.; Liu, J.; Liu, J.-P. Pulmonary
772 Alveolar Stem Cell Senescence, Apoptosis, and Differentiation by P53-Dependent and -

773 Independent Mechanisms in Telomerase-Deficient Mice. *Cells* **2021**, *10* (11).
774 https://doi.org/10.3390/cells10112892.

775 (23) Yasutomo, K. Genetics and Animal Models of Familial Pulmonary Fibrosis. *Int Immunol*
776 **2021**, *33* (12), 653–657. https://doi.org/10.1093/intimm/dxab026.

777 (24) Wernig, G.; Chen, S.-Y.; Cui, L.; Van Neste, C.; Tsai, J. M.; Kambham, N.; Vogel, H.;
778 Natkunam, Y.; Gilliland, D. G.; Nolan, G.; Weissman, I. L. Unifying Mechanism for
779 Different Fibrotic Diseases. *Proceedings of the National Academy of Sciences* **2017**, *114*
780 (18), 4757–4762. https://doi.org/10.1073/pnas.1621375114.

781 (25) Malara, A.; Abbonante, V.; Zingariello, M.; Migliaccio, A.; Balduini, A. Megakaryocyte
782 Contribution to Bone Marrow Fibrosis: Many Arrows in the Quiver. *Mediterr J Hematol*
783 *Infect Dis* **2018**, *10* (1), e2018068–e2018068. https://doi.org/10.4084/MJHID.2018.068.

784 (26) Tefferi, A. Primary Myelofibrosis: 2023 Update on Diagnosis, Risk-stratification, and
785 Management. *Am J Hematol* **2023**, *98* (5), 801–821. https://doi.org/10.1002/ajh.26857.

786 (27) Passamonti, F.; Mora, B. Myelofibrosis. *Blood* **2022**.
787 https://doi.org/10.1182/blood.2022017423.

788 (28) Jeremy Wen, Q.; Yang, Q.; Goldenson, B.; Malinge, S.; Lasho, T.; Schneider, R. K.;
789 Breyfogle, L. J.; Schultz, R.; Gilles, L.; Koppikar, P.; Abdel-Wahab, O.; Pardanani, A.;
790 Stein, B.; Gurbuxani, S.; Mullally, A.; Levine, R. L.; Tefferi, A.; Crispino, J. D. Targeting
791 Megakaryocytic-Induced Fibrosis in Myeloproliferative Neoplasms by AURKA Inhibition.
792 *Nat Med* **2015**, *21* (12), 1473–1480. https://doi.org/10.1038/nm.3995.

793 (29) Ciurea, S. O.; Merchant, D.; Mahmud, N.; Ishii, T.; Zhao, Y.; Hu, W.; Bruno, E.; Barosi,
794 G.; Xu, M.; Hoffman, R. Pivotal Contributions of Megakaryocytes to the Biology of
795 Idiopathic Myelofibrosis. *Blood* **2007**, *110* (3), 986–993. https://doi.org/10.1182/blood-
796 2006-12-064626.

797 (30) Gilles, L.; Arslan, A. D.; Marinaccio, C.; Wen, Q. J.; Arya, P.; McNulty, M.; Yang, Q.;
798 Zhao, J. C.; Konstantinoff, K.; Lasho, T.; Pardanani, A.; Stein, B.; Plo, I.; Sundaravel, S.;
799 Wickrema, A.; Migliaccio, A.; Gurbuxani, S.; Vainchenker, W.; Platanias, L. C.; Tefferi,
800 A.; Crispino, J. D. Downregulation of GATA1 Drives Impaired Hematopoiesis in Primary
801 Myelofibrosis. *J Clin Invest* **2017**, *127* (4), 1316–1320. https://doi.org/10.1172/JCI82905.

802 (31) Vannucchi, A. M.; Pancrazzi, A.; Guglielmelli, P.; Di Lollo, S.; Bogani, C.; Baroni, G.;
803 Bianchi, L.; Migliaccio, A. R.; Bosi, A.; Paoletti, F. Abnormalities of GATA-1 in
804 Megakaryocytes from Patients with Idiopathic Myelofibrosis. *Am J Pathol* **2005**, *167* (3),
805 849–858. https://doi.org/10.1016/S0002-9440(10)62056-1.

806 (32) Shivdasani, R. A.; Orkin, S. H. The Transcriptional Control of Hematopoiesis. *Blood* **1996**,
807 *87* (10), 4025–4039. https://doi.org/10.1182/blood.V87.10.4025.bloodjournal87104025.

808 (33) Shivdasani, R. A.; Fujiwara, Y.; McDevitt, M. A.; Orkin, S. H. A Lineage-Selective
809 Knockout Establishes the Critical Role of Transcription Factor GATA-1 in Megakaryocyte
810 Growth and Platelet Development. *EMBO Journal* **1997**, *16* (13), 3965–3973.
811 https://doi.org/10.1093/emboj/16.13.3965.

812 (34) Vannucchi, A. M.; Bianchi, L.; Cellai, C.; Paoletti, F.; Rana, R. A.; Lorenzini, R.;
813 Migliaccio, G.; Migliaccio, A. R. Development of Myelofibrosis in Mice Genetically
814 Impaired for GATA-1 Expression (GATA-1(Low) Mice). *Blood* **2002**, *100* (4), 1123–1132.
815 https://doi.org/10.1182/blood-2002-06-1913.

816 (35) Zingariello, M.; Martelli, F.; Ciaffoni, F.; Masiello, F.; Ghinassi, B.; D'Amore, E.; Massa,
817 M.; Barosi, G.; Sancillo, L.; Li, X.; Goldberg, J. D.; Rana, R. A.; Migliaccio, A. R.
818 Characterization of the TGF-Beta1 Signaling Abnormalities in the Gata1low Mouse Model
819 of Myelofibrosis. *Blood* **2013**, *121* (17), 3345–3363. https://doi.org/10.1182/blood-2012-
820 06-439661.

821 (36) Zingariello, M.; Verachi, P.; Gobbo, F.; Martelli, F.; Falchi, M.; Mazzarini, M.; Valeri, M.;
822 Sarli, G.; Marinaccio, C.; Melo-Cardenas, J.; Crispino, J. D.; Migliaccio, A. R. Resident
823 Self-Tissue of Proinflammatory Cytokines Rather Than Their Systemic Levels Correlates
824 with Development of Myelofibrosis in Gata1low Mice. *Biomolecules*. 2022.
825 https://doi.org/10.3390/biom12020234.

826 (37) Spangrude, G. J.; Lewandowski, D.; Martelli, F.; Marra, M.; Zingariello, M.; Sancillo, L.;
827 Rana, R. A.; Migliaccio, A. R. P-Selectin Sustains Extramedullary Hematopoiesis in the
828 Gata1low Model of Myelofibrosis. *Stem Cells* **2016**, *34* (1), 67–82.
829 https://doi.org/10.1002/stem.2229.

830 (38) Lefrançais, E.; Ortiz-Muñoz, G.; Caudrillier, A.; Mallavia, B.; Liu, F.; Sayah, D. M.;
831 Thornton, E. E.; Headley, M. B.; David, T.; Coughlin, S. R.; Krummel, M. F.; Leavitt, A.
832 D.; Passegué, E.; Looney, M. R. The Lung Is a Site of Platelet Biogenesis and a Reservoir
833 for Haematopoietic Progenitors. *Nature* **2017**, *544* (7648), 105–109.
834 https://doi.org/10.1038/nature21706.

835 (39) Trowbridge, E. A.; Martin, J. F.; Slater, D. N. Evidence for a Theory of Physical
836 Fragmentation of Megakaryocytes, Implying That All Platelets Are Produced in the
837 Pulmonary Circulation. *Thromb Res* **1982**, *28* (4), 461–475.
838 https://doi.org/https://doi.org/10.1016/0049-3848(82)90163-3.

839 (40) Pariser, D. N.; Hilt, Z. T.; Ture, S. K.; Blick-Nitko, S. K.; Looney, M. R.; Cleary, S. J.;
840 Roman-Pagan, E.; II, J. S.; Georas, S. N.; Veazey, J.; Madere, F.; Santos, L. T.; Arne, A.;
841 Huynh, N. P. T.; Livada, A. C.; Guerrero-Martin, S. M.; Lyons, C.; Metcalf-Pate, K. A.;
842 McGrath, K. E.; Palis, J.; Morrell, C. N. Lung Megakaryocytes Are Immune Modulatory
843 Cells. *J Clin Invest* **2021**, *131* (1). https://doi.org/10.1172/JCI137377.

844 (41) Yeung, A. K.; Villacorta-Martin, C.; Hon, S.; Rock, J. R.; Murphy, G. J. Lung
845 Megakaryocytes Display Distinct Transcriptional and Phenotypic Properties. *Blood Adv*
846 **2020**, *4* (24), 6204–6217. https://doi.org/10.1182/bloodadvances.2020002843.

847 (42) Wang, H.; He, J.; Xu, C.; Chen, X.; Yang, H.; Shi, S.; Liu, C.; Zeng, Y.; Wu, D.; Bai, Z.;
848 Wang, M.; Wen, Y.; Su, P.; Xia, M.; Huang, B.; Ma, C.; Bian, L.; Lan, Y.; Cheng, T.; Shi,
849 L.; Liu, B.; Zhou, J. Decoding Human Megakaryocyte Development. *Cell Stem Cell* **2021**,
850 *28* (3), 535-549.e8. https://doi.org/10.1016/j.stem.2020.11.006.

851 (43) Sun, S.; Jin, C.; Si, J.; Lei, Y.; Chen, K.; Cui, Y.; Liu, Z.; Liu, J.; Zhao, M.; Zhang, X.;
852 Tang, F.; Rondina, M. T.; Li, Y.; Wang, Q.-F. Single-Cell Analysis of Ploidy and the
853 Transcriptome Reveals Functional and Spatial Divergency in Murine Megakaryopoiesis.
854 *Blood* **2021**, *138* (14), 1211–1224. https://doi.org/10.1182/blood.2021010697.

855 (44) Zhou, Y.; Zhang, B.; Li, C.; Huang, X. T.; Cheng, H. P.; Bao, X. W.; Zhao, F. Y.; Cheng,
856 Q. M.; Yue, S. J.; Han, J. Z.; Luo, Z. Q. Megakaryocytes Participate in the Occurrence of
857 Bleomycin-Induced Pulmonary Fibrosis. *Cell Death Dis* **2019**, *10* (9), 648.
858 https://doi.org/10.1038/s41419-019-1903-8.

859 (45) Brayton, C. F.; Treuting, P. M.; Ward, J. M. Pathobiology of Aging Mice and GEM. *Vet*
860 *Pathol* **2012**, *49* (1), 85–105. https://doi.org/10.1177/0300985811430696.

861 (46) Crooks, M. G.; Fahim, A.; Naseem, K. M.; Morice, A. H.; Hart, S. P. Increased Platelet
862 Reactivity in Idiopathic Pulmonary Fibrosis Is Mediated by a Plasma Factor. *PLoS One*
863 **2014**, *9* (10), e111347. https://doi.org/10.1371/journal.pone.0111347.

864 (47) Kass, D. J.; Nouraie, M.; Glassberg, M. K.; Ramreddy, N.; Fernandez, K.; Harlow, L.;
865 Zhang, Y.; Chen, J.; Kerr, G. S.; Reimold, A. M.; England, B. R.; Mikuls, T. R.; Gibson, K.
866 F.; Dellaripa, P. F.; Rosas, I. O.; Oddis, C. V.; Ascherman, D. P. Comparative Profiling of
867 Serum Protein Biomarkers in Rheumatoid Arthritis–Associated Interstitial Lung Disease
868 and Idiopathic Pulmonary Fibrosis. *Arthritis & Rheumatology* **2020**, *72* (3), 409–419.
869 https://doi.org/10.1002/art.41123.

870 (48) Guiot, J.; Moermans, C.; Henket, M.; Corhay, J.-L.; Louis, R. Blood Biomarkers in
871 Idiopathic Pulmonary Fibrosis. *Lung* **2017**, *195* (3), 273–280.
872 https://doi.org/10.1007/s00408-017-9993-5.

873 (49) Papiris, S. A.; Tomos, I. P.; Karakatsani, A.; Spathis, A.; Korbila, I.; Analitis, A.; Kolilekas,
874 L.; Kagouridis, K.; Loukides, S.; Karakitsos, P.; Manali, E. D. High Levels of IL-6 and IL-
875 8 Characterize Early-on Idiopathic Pulmonary Fibrosis Acute Exacerbations. *Cytokine*
876 **2018**, *102*, 168–172. https://doi.org/10.1016/j.cyto.2017.08.019.

877 (50) Khalil, N.; O'Connor, R. The Role of TGF-β in Bleomycin Induced Pulmonary Fibrosis BT
878 - Transforming Growth Factor-β in Cancer Therapy. *Humana Press:Totowa, N* **2008**.

879 (51) Chen, X.; Shi, C.; Meng, X.; Zhang, K.; Li, X.; Wang, C.; Xiang, Z.; Hu, K.; Han, X.
880 Inhibition of Wnt/β-Catenin Signaling Suppresses Bleomycin-Induced Pulmonary Fibrosis
881 by Attenuating the Expression of TGF-B1 and FGF-2. *Exp Mol Pathol* **2016**, *101* (1), 22–
882 30. https://doi.org/10.1016/j.yexmp.2016.04.003.

883 (52) Saito, A.; Horie, M.; Micke, P.; Nagase, T. The Role of TGF-β Signaling in Lung Cancer
884 Associated with Idiopathic Pulmonary Fibrosis. *Int J Mol Sci* **2018**, *19* (11), 3611.
885 https://doi.org/10.3390/ijms19113611.

886 (53) Khalil, N.; Corne, S.; Whitman, C.; Yacyshyn, H. Plasmin Regulates the Activation of Cell-
887 Associated Latent TGF-Beta 1 Secreted by Rat Alveolar Macrophages after in Vivo

888 Bleomycin Injury. *Am J Respir Cell Mol Biol* **1996**, *15* (2), 252–259.
889 https://doi.org/10.1165/ajrcmb.15.2.8703482.

890 (54) Khalil, N.; O'Connor, R. N.; Unruh, H. W.; Warren, P. W.; Flanders, K. C.; Kemp, A.;
891 Bereznay, O. H.; Greenberg, A. H. Increased Production and Immunohistochemical
892 Localization of Transforming Growth Factor- α in Idiopathic Pulmonary Fibrosis. *Am J*
893 *Respir Cell Mol Biol* **1991**, *5* (2), 155–162. https://doi.org/10.1165/ajrcmb/5.2.155.

894 (55) Xu, Y. D.; Hua, J.; Mui, A.; O'Connor, R.; Grotendorst, G.; Khalil, N. Release of
895 Biologically Active TGF-B1 by Alveolar Epithelial Cells Results in Pulmonary Fibrosis.
896 *American Journal of Physiology-Lung Cellular and Molecular Physiology* **2003**, *285* (3),
897 L527–L539. https://doi.org/10.1152/ajplung.00298.2002.

898 (56) Liang, J.; Huang, G.; Liu, X.; Taghavifar, F.; Liu, N.; Yao, C.; Deng, N.; Wang, Y.; Burman,
899 A.; Xie, T.; Rowan, S.; Chen, P.; Hogaboam, C.; Stripp, B.; Weigt, S. S.; Belperio, J.; Parks,
900 W. C.; Noble, P. W.; Jiang, D. Single-Cell Transcriptomics Identifies Dysregulated
901 Metabolic Programs of Aging Alveolar Progenitor Cells in Lung Fibrosis. *bioRxiv* **2020**,
902 2020.07.30.227892. https://doi.org/10.1101/2020.07.30.227892.

903 (57) Izbicki, G.; Segel, M. J.; Christensen, T. G.; Conner, M. W.; Breuer, R. Time Course of
904 Bleomycin-Induced Lung Fibrosis. *Int J Exp Pathol* **2002**, *83* (3), 111–119.
905 https://doi.org/10.1046/j.1365-2613.2002.00220.x.

906 (58) Redente, E. F.; Jacobsen, K. M.; Solomon, J. J.; Lara, A. R.; Faubel, S.; Keith, R. C.;
907 Henson, P. M.; Downey, G. P.; Riches, D. W. H. Age and Sex Dimorphisms Contribute to
908 the Severity of Bleomycin-Induced Lung Injury and Fibrosis. *American Journal of*
909 *Physiology-Lung Cellular and Molecular Physiology* **2011**, *301* (4), L510–L518.
910 https://doi.org/10.1152/ajplung.00122.2011.

911 (59) Khalil, N.; O'Connor, R. N.; Flanders, K. C.; Unruh, H. TGF-Beta 1, but Not TGF-Beta 2
912 or TGF-Beta 3, Is Differentially Present in Epithelial Cells of Advanced Pulmonary
913 Fibrosis: An Immunohistochemical Study. *Am J Respir Cell Mol Biol* **1996**, *14* (2), 131–
914 138. https://doi.org/10.1165/ajrcmb.14.2.8630262.

915 (60) Cheng, Y.; Ma, X.; Wei, Y.; Wei, X.-W. Potential Roles and Targeted Therapy of the
916 CXCLs/CXCR2 Axis in Cancer and Inflammatory Diseases. *Biochimica et Biophysica Acta*

917 *(BBA) - Reviews on Cancer* **2019**, *1871* (2), 289–312.
918 https://doi.org/10.1016/j.bbcan.2019.01.005.

919 (61) Liu, Q.; Li, A.; Tian, Y.; Wu, J. D.; Liu, Y.; Li, T.; Chen, Y.; Han, X.; Wu, K. The CXCL8-
920 CXCR1/2 Pathways in Cancer. *Cytokine Growth Factor Rev* **2016**, *31*, 61–71.
921 https://doi.org/10.1016/j.cytogfr.2016.08.002.

922 (62) Mei, J.; Liu, Y.; Dai, N.; Favara, M.; Greene, T.; Jeyaseelan, S.; Poncz, M.; Lee, J. S.;
923 Worthen, G. S. CXCL5 Regulates Chemokine Scavenging and Pulmonary Host Defense to
924 Bacterial Infection. *Immunity* **2010**, *33* (1), 106–117.
925 https://doi.org/10.1016/j.immuni.2010.07.009.

926 (63) Elemam, N.; Talaat, I.; Maghazachi, A. CXCL10 Chemokine: A Critical Player in RNA
927 and DNA Viral Infections. *Viruses* **2022**, *14* (11), 2445. https://doi.org/10.3390/v14112445.

928 (64) Cheng, I.-Y.; Liu, C.-C.; Lin, J.-H.; Hsu, T.-W.; Hsu, J.-W.; Li, A. F.-Y.; Ho, W.-C.; Hung,
929 S.-C.; Hsu, H.-S. Particulate Matter Increases the Severity of Bleomycin-Induced
930 Pulmonary Fibrosis through KC-Mediated Neutrophil Chemotaxis. *Int J Mol Sci* **2019**, *21*
931 (1), 227. https://doi.org/10.3390/ijms21010227.

932 (65) Mattos, M. S.; Ferrero, M. R.; Kraemer, L.; Lopes, G. A. O.; Reis, D. C.; Cassali, G. D.;
933 Oliveira, F. M. S.; Brandolini, L.; Allegretti, M.; Garcia, C. C.; Martins, M. A.; Teixeira,
934 M. M.; Russo, R. C. CXCR1 and CXCR2 Inhibition by Ladarixin Improves Neutrophil-
935 Dependent Airway Inflammation in Mice. *Front Immunol* **2020**, *11*.
936 https://doi.org/10.3389/fimmu.2020.566953.

937 (66) Ferrari, A.; Scandura, J.; Masciulli, A.; Krichevsky, S.; Gavazzi, A.; Barbui, T. Prevalence
938 and Risk Factors for Pulmonary Hypertension Associated with Chronic Myeloproliferative
939 Neoplasms. *Eur J Haematol* **2021**, *106* (2), 250–259. https://doi.org/10.1111/ejh.13543.

940 (67) Young, N. S.; Scheinberg, P.; Calado, R. T. Aplastic Anemia. *Curr Opin Hematol* **2008**, *15*
941 (3), 162–168. https://doi.org/10.1097/MOH.0b013e3282fa7470.

942 (68) Meng, Y.; Carrelha, J.; Drissen, R.; Ren, X.; Zhang, B.; Gambardella, A.; Valletta, S.;
943 Thongjuea, S.; Jacobsen, S. E.; Nerlov, C. Epigenetic Programming Defines
944 Haematopoietic Stem Cell Fate Restriction. *Nat Cell Biol* **2023**.
945 https://doi.org/10.1038/s41556-023-01137-5.

946 (69) Hashimoto, N.; Jin, H.; Liu, T.; Chensue, S. W.; Phan, S. H. Bone Marrow–Derived
947 Progenitor Cells in Pulmonary Fibrosis. *Journal of Clinical Investigation* **2004**, *113* (2),
948 243–252. https://doi.org/10.1172/JCI200418847.

949 (70) Dunsmore, S. E.; Shapiro, S. D. The Bone Marrow Leaves Its Scar: New Concepts in
950 Pulmonary Fibrosis. *Journal of Clinical Investigation* **2004**, *113* (2), 180–182.
951 https://doi.org/10.1172/JCI20782.

952 (71) Spangrude, G. J.; Lewandowski, D.; Martelli, F.; Marra, M.; Zingariello, M.; Sancillo, L.;
953 Rana, R. A.; Migliaccio, A. R. P-Selectin Sustains Extramedullary Hematopoiesis in the
954 Gata1low Model of Myelofibrosis. *Stem Cells* **2016**, *34* (1), 67–82.
955 https://doi.org/10.1002/stem.2229.

956 (72) Embury, S. H.; Matsui, N. M.; Ramanujam, S.; Mayadas, T. N.; Noguchi, C. T.; Diwan, B.
957 A.; Mohandas, N.; Cheung, A. T. W. The Contribution of Endothelial Cell P-Selectin to the
958 Microvascular Flow of Mouse Sickle Erythrocytes in Vivo. *Blood* **2004**, *104* (10), 3378–
959 3385. https://doi.org/10.1182/blood-2004-02-0713.

960 (73) Verachi, P.; Gobbo, F.; Martelli, F.; Falchi, M.; di Virgilio, A.; Sarli, G.; Wilke, C.;
961 Bruederle, A.; Prahallad, A.; Arciprete, F.; Zingariello, M.; Migliaccio, A. R. Preclinical
962 Studies on the Use of a P-Selectin-Blocking Monoclonal Antibody to Halt Progression of
963 Myelofibrosis in the Gata1 Mouse Model. *Exp Hematol* **2022**.
964 https://doi.org/10.1016/j.exphem.2022.09.004.

965 (74) Varricchio, L.; Iancu-Rubin, C.; Upadhyaya, B.; Zingariello, M.; Martelli, F.; Verachi, P.;
966 Clementelli, C.; Denis, J.-F.; Rahman, A. H.; Tremblay, G.; Mascarenhas, J.; Mesa, R. A.;
967 O'Connor-McCourt, M.; Migliaccio, A. R.; Hoffman, R. TGF-B1 Protein Trap AVID200
968 Beneficially Affects Hematopoiesis and Bone Marrow Fibrosis in Myelofibrosis. *JCI*
969 *Insight* **2021**, *6* (18). https://doi.org/10.1172/jci.insight.145651.

970 (75) Dunbar, A.; Kim, D.; Lu, M.; Farina, M.; Bowman, R. L.; Yang, J. L.; Park, Y. C.; Karzai,
971 A.; Xiao, W.; Zaroogian, Z.; O'Connor, K.; Mowla, S.; Gobbo, F.; Verachi, P.; Martelli, F.;
972 Sarli, G.; Xia, L.; Elmansy, N.; Kleppe, M.; Chen, Z.; Xiao, Y.; McGovern, E. M.; Snyder,
973 J.; Krishnan, A.; Hill, C. E.; Cordner, K. B.; Zouak, A.; Salama, M. E.; Yohai, J.; Tucker,
974 E.; Chen, J. J.; Zhou, J.; McConnell, T. S.; Migliaccio, A. R.; Koche, R. P.; Rampal, R. K.;

975 Fan, R.; Levine, R. L.; Hoffman, R. CXCL8/CXCR2 Signaling Mediates Bone Marrow
976 Fibrosis and Represents a Therapeutic Target in Myelofibrosis. *Blood* **2023**.
977 https://doi.org/10.1182/blood.2022015418.

978 (76) Verachi, P.; Gobbo, F.; Martelli, F.; Martinelli, A.; Sarli, G.; Dunbar, A.; Levine, R. L.;
979 Hoffman, R.; Massucci, M. T.; Brandolini, L.; Giorgio, C.; Allegretti, M.; Migliaccio, A.
980 R. The CXCR1/CXCR2 Inhibitor Reparixin Alters the Development of Myelofibrosis in
981 the Gata1low Mice. *Front Oncol* **2022**, *12*. https://doi.org/10.3389/fonc.2022.853484.

982 (77) Yu, G.; Wang, L.-G.; Yan, G.-R.; He, Q.-Y. DOSE: An R/Bioconductor Package for
983 Disease Ontology Semantic and Enrichment Analysis. *Bioinformatics* **2015**, *31* (4), 608–
984 609. https://doi.org/10.1093/bioinformatics/btu684.

985 (78) Yu, G.; Wang, L.-G.; Han, Y.; He, Q.-Y. ClusterProfiler: An R Package for Comparing
986 Biological Themes Among Gene Clusters. *OMICS* **2012**, *16* (5), 284–287.
987 https://doi.org/10.1089/omi.2011.0118.

988 (79) Wu, T.; Hu, E.; Xu, S.; Chen, M.; Guo, P.; Dai, Z.; Feng, T.; Zhou, L.; Tang, W.; Zhan, L.;
989 Fu, X.; Liu, S.; Bo, X.; Yu, G. ClusterProfiler 4.0: A Universal Enrichment Tool for
990 Interpreting Omics Data. *The Innovation* **2021**, *2* (3), 100141.
991 https://doi.org/10.1016/j.xinn.2021.100141.

992

993

994

995

996

997

998

999

1000 **Figure Legends**

1001 **Figure 1. The lung from patients with IPF contains numerous GATA1 hypomorphic**
1002 **megakaryocytes biased for the immune lineage.** (A) First line: Double IF staining with anti-
1003 GATA1 (green) and CD42b (red, as a marker of MK) of lung sections from one IPF and one
1004 representative no-IPF patient, as indicated. Nuclei are counterstained with DAPI. The inserts show
1005 representative MK at high power fields. The signal captured in the individual channels are
1006 presented in **Figure S1**. Second and third lines: Hematoxilin&Eosin (H&E) and reticulin staining
1007 of the corresponding consecutive sections confirming that the lung from the IPF patient has an
1008 overall abnormal architecture with fibrosis. Magnification 400x in the panels on the top and 200x
1009 in the middle and bottom panels. (B) Frequency of CD42b^{pos} MK per area (0.488mm^2) and
1010 percentage of GATA1^{pos} MK (over the total number of CD42b^{pos} cells) observed in the lungs from
1011 IPF and no-IPF patients, as indicated. Data are presented as Mean(±SD) and as value in individual
1012 subjects (each dot represents a single subject). The data are analyzed by One-way ANOVA and
1013 significant p values are indicated within the panels. C) Confocal microscopy analyses for markers
1014 of immune (CD41, green/LSP1, red), HSC-supporting (CD61 green/MYLK4 red) and Plt-poised
1015 (CD42b red/ARNTL green) MK in the lung from a representative no-IPF and a IPF patients, as
1016 indicated. Signals are presented in the individual channel and merged mode. The signals in the
1017 green and red channel are presented individually and in combination. Original Magnification 400x.
1018 D-F) Frequency of total CD41pos and CD41pos/LPS1pos (immune-MK. D), CD61pos and
1019 CD61pos/MYLKpos (HSC-supporting MK, E) and total CD42b^{pos} and CD42b^{pos}/ARNTL^{pos} (Plt-
1020 MK, F) MK detected in the lungs from three representative No-IPF and three IPF patients, as
1021 indicated. Data are presented as Mean(±SD) and as value in individual subjects (each dot
1022 represents a single subject). The data are analyzed by One-way ANOVA and significant p values
1023 are indicated within the panels.

1024 **Figure 2. The megakaryocytes in the lungs from *Gata1^{low}* mice are immature and with age**
1025 **became biased for the immune-lineage and express a defective immune-signature.** (A) IHC
1026 with the CD42b antibody of lung sections from WT (wild-type) and *Gata1*^{low} littermates, as well
1027 as from *P-sel*^{null} and *P-sel*^{null}*Gata1*^{low} mice used as additional controls, as indicated. The panels
1028 present representative immature (MK) and mature Plt-forming (PfMK) MK found in the different
1029 groups. Scale bar 50µm. Magnification See Figure S2A for further detail. (*B*) Confocal microscopy

1030 analysis for CD42b (red) and GATA1 (green) of the MK in the lung from representative *Gata1*^{low}
1031 and WT littermates. Original Magnification 400x. The signal captured in the individual channels
1032 are presented in **Figure S2B**. The frequency of CD42b^{pos} MK per area (0.488mm^2) and the
1033 percentage of GATA1^{pos} MK (over the total number of CD42b^{pos} cells) observed in the lungs from
1034 multiple mice is presented as Mean(±SD) and as value in individual mice (each dot represents a
1035 single mouse). The data are analyzed by One-way ANOVA and significant p values are indicated
1036 within the panels. C) Frequency of CD42b^{pos} cells with a DNA content 2N, 4N and >8N in lungs
1037 from *Gata1*^{low} mice and WT littermates (both 15-months old) determined by Flow cytometry, as
1038 indicated. Data are presented as Mean (±SD) and as value in individual mice (each symbol a single
1039 mouse) and were analyzed by ANOVA. Statistically significant p values are indicated within the
1040 panels. D) Confocal microscopy analyses for markers of immune (CD41, green/LSP1, red), HSC-
1041 supporting MK (CD61 green/MYLK4 red) and Plt-poised (CD42b red/ARNTL green) MK in the
1042 lung from representative WT and *Gata1*^{low} mice at 2-3 (young) and 15-months (old) of age, as
1043 indicated. Original Magnification 40x. The signal captured in the individual channels are presented
1044 in **Figure S4**. E-G) Frequency of total CD41pos and CD41pos/LPS1pos (immune-MK, E),
1045 CD61pos and CD61pos/MYLKpos (HSC-supporting MK, F) and total CD42b^{pos} and
1046 CD42b^{pos}/ARNTL^{pos} (Plt-MK, G) MK detected in the lungs from multiple young and old WT and
1047 *Gata1*^{low} mice. Data are presented as Mean(±SD) and as value in individual subjects (each dot
1048 represents a single mouse). The data are analyzed by One-way ANOVA and significant p values
1049 are indicated within the panels. **H)** Principal component analysis (PCA**)** of the RNAseq data
1050 obtained with MK purified from the BM and lungs of individual 15-months old WT and *Gata1*^{low}
1051 littermates (each dot an individual mouse) as indicated. The strong separation and clustering of
1052 samples demonstrates the high reproducibility of the data from the same group. The differences
1053 between tissue of provenience (BM or lung) account for approximately 79% of the variance in the
1054 data. **I)** Log ratio vs mean average (MA) plot of up- and down-regulated genes in MK from the
1055 lungs of *Gata1*^{low} mice lungs with respect to the MK from WT lungs. **F)** Heatmaps for the level of
1056 expression of representative genes which characterize the signature of immune (blue), HSC-
1057 supporting (green) and Plt-poised (red) MK described by[43] . Statistically significant ($p<0.05$)
1058 differences are indicated by asterisks. Interestingly, in spite of the fact that the lungs from Gata1^{low}
1059 mice are enriched for immune-MK, they have an overall defective immune-signature.

1060 **Figure 3. Although inflammation is present in lungs from young and old wild-type and**
1061 ***Gata1*^{low} littermates alike, fibrosis is present only in those from old *Gata1*^{low} mice.** (A) Stack
1062 images of the lungs from representative WT and *Gata1*^{low} littermates (both 20 months old) stained
1063 by H&E or Masson's trichrome, as indicated. Original magnification 40x. Abbreviations:
1064 cr=cranial: cd=caudal; d=; l=lateral and m=medial. B) H&E staining of sections of the lungs from
1065 representative WT and *Gata1*^{low} littermates expressing interstitial pneumonia at grade 0, 1, 2 and
1066 3, as indicated. Red and green arrows indicate lymphocytes and neutrophils respectively.
1067 Magnification 200x. The frequency of mice found to express the different grades of inflammation
1068 in the two groups is indicated on the right. C) H&E, Reticulin and Masson's trichrome staining of
1069 consecutive sections from the lungs of representative WT and *Gata1*^{low} littermates, as indicated.
1070 Magnification 100x. D-F) Quantification of fibrosis by reticulin staining (D) and association of
1071 fibrosis evaluated by Masson's trichrome staining with age (E) and sex (F) in the lung, stratified
1072 by WT, *Gata1*^{low}, *P-sel*^{null} and *Gata1*^{low}*P-sel*^{null} littermates, as indicated. P-values from One-way
1073 ANOVA (D) and simple linear (E) or logistic (F) regression models, stratified by genotype are
1074 overlayed, along with p-value for the interaction term from a multivariable model including age
1075 and genotype (E) or sex and genotype (F) as covariates (see **Table 1** for further detail).

1076 **Figure 4. Lungs from old *Gata1*^{low} mice contain levels greater than normal of P-SEL, TGF-**
1077 **β1 and CXCL1 which are specifically accumulated in cells with a megakaryocyte**
1078 **morphology.** A) Immunohistochemical staining for P-SEL, TGF-β1 and CXCL1 of lung sections
1079 from representative WT, *Gata1*^{low}, *P-sel*^{null} and *Gata1*^{low}*P-sel*^{null} mice (8-24 months old), as
1080 indicated. Magnification 200x. B) Quantification by computer assisted imaging of the P-SEL,
1081 TGF-β1 and CXCL1 content in the lungs from the four experimental groups. Data are presented
1082 as Mean(±SD) and were analyzed by Tukey's multiple comparisons test. Values observed in
1083 individual mice are presented as dots. Statistically significant p values (<0.05) among groups are
1084 indicated withing the panels. C) P-SEL, TGF-β1 and CXCL1 content in endothelial cells, Type II
1085 pneumocytes, bronchial epithelium, macrophages, neutrophils and MK from representative WT
1086 and *Gata1*^{low} littermates (both 13-months old) as indicated. Cells were identified according to the
1087 following morphological criteria: Endothelial cells were recognized as flat cells delimiting the
1088 vessels lumina; Type II pneumocytes were identified as cuboidal cells intermingled to flat cells
1089 (Type I pneumocytes) along alveolar walls; Bronchial epithelium as pseudostratified to mono-
1090 stratified cuboidal cells along airways; macrophages as cells with round nucleus and abundant

1091 cytoplasm; neutrophils on the basis of their small size (9μm) and kidney shaped nuclei and MK on
1092 the basis of their size (10 times greater than that of any other cell type) and the polylobate
1093 morphology of their nuclei. Magnification 400x. Semi-quantitative estimates of protein content
1094 are indicated as undetectable (-), present (+) and strongly present (++).

1095 **Figure 5. Development of fibrosis in the lung from *Gata1^{low}* mice is prevented by genetic**
1096 **ablation of *P-selectin* and is rescued by treatments with inhibitors of either P-selectin, TGF-**
1097 **β or CXCR1/2.** A) H&E, Reticulin and Masson's trichrome staining of consecutive sections of
1098 lungs from representative WT, *Gata1*^{low}, *P-sel*^{null} and *P-sel*^{null}*Gata1*^{low} mice (all 12-15 months
1099 old), as indicated. Magnification 40x. Results observed in multiple mice per experimental group
1100 are presented and analyzed in detail in **Figure 2** and **Table 1**. B, E and H) H&E, Reticulin and
1101 Masson's trichrome staining of consecutive sections from lungs of representative *Gata1*^{low} mice
1102 treated with either vehicle or the P-SEL antibody for 5, 12 or 40 days (B), with either vehicle or
1103 the TGF-β inhibitor for 5 or 10 weeks (E) or either with vehicle or the CXCR1/2inhibitor for 20
1104 or 37 days. H), as indicated. Magnification 200x. C, F and I) Number of *Gata1*^{low} mice (in percent
1105 of the total) expressing Grade 0, 1, 2 or 3 of inflammation when treated with either vehicle or the
1106 P-SEL inhibitor C), or when treated either with vehicle or the TGF-β (F) or either with vehicle or
1107 the CXCR1/2 inhibitor (I). Results of the vehicle groups at different time points were pooled,
1108 because similar. D, G, J) Level of fibrosis detected by reticulin or Masson staining in consecutive
1109 lung sections from mice treated either with vehicle or with the P-SEL inhibitor (D), either with
1110 vehicle or the TGF-β inhibitor (G). or either with vehicle or the CXCR1/2 inhibitor (J). Data are
1111 presented as Mean (±SD) and as data per individual mouse (each dot a single mouse). Statistical
1112 analyses were performed were by one-way ANOVA and p values statistically significant between
1113 groups are indicated within the panels.

1114 **Figure 6. In the lung from *Gata1^{low}* mice, treatment with the P-SEL inhibitor reduces the**
1115 **content of both TGF-β1 and CXCL1 and increases that of GATA1 of the megakaryocytes**
1116 **while those with either the TGF-β1 or the CXCR12 inhibitor reduce the levels of CXCL1**
1117 **only.** A) Immunohistochemical staining for TGF-β1 and CXCL1 of consecutive lung sections
1118 from representative *Gata1*^{low} mice treated either with vehicle (one mouse representative of the
1119 vehicle group for all the treatments) or with the P-SEL (day 12 and 40), TGF-β1 (5 and 10 weeks)
1120 or CXCR1/2 (20 or 37 days) inhibitor, as indicated. Magnification 400x. B,C) Quantification of
1121 the TGF-β1 (B) and CXCL1 (C) content of lungs from *Gata1*^{low} mice treated either with vehicle

1122 or inhibitors for P-SEL, TGF-β1 or CXCR1/2, as indicated. Data are presented as Mean (±SD) and
1123 as values per individual mice (each symbol a different mouse) and were analyzed by one-way
1124 Anova. P values statistically significant are indicated within the panels. D) Double immune-
1125 fluorescence staining with anti-GATA1 (green) and CD42b (red as a marker of MK) of lung
1126 sections from representative *Gata1*^{low} mice treated either with vehicle or inhibitors for either P-
1127 SEL (day 12 and 40), TGF-β1 (5 and 10 weeks) or CXCLR1/2 (20 or 37 days), as indicated. Nuclei
1128 were highlighted with DAPI (blue). Magnification 400x. The signal captured in the individual
1129 channels are presented in **Figure S10**. E) Total number of MK (CD42b^{pos} cells) and of MK
1130 expressing detectable levels of GATA1 in the lungs from *Gata1*^{low} mice treated either with vehicle
1131 or the P-SEL, TGF-β1 or CXCR1/2 inhibitor, as indicated. Data are presented as Mean (±SD) and
1132 as values per individual mice (each symbol a different mouse) and were analyzed by one-way
1133 Anova. P values statistically significant are indicated within the panels.
1134

Table 1: Comparison of age, sex, and histological parameters between *Gata1*^{low} mice vs WT and *Gata1*^{low} mice vs P-sel^{null}Gata1^{low}

	Gata1^{low} (n=47)	WT (n=18)	Unadjusted p-value	Age-adjusted p-value	Sex-adjusted p-value	P-sel^{null}Gata1^{low} (n=25)	Unadjusted p-value	Age-adjusted p-value	Sex-adjusted p-value
Age (months)			0.01[a]				0.07[a]		
N (Missing)	47 (0)	18 (0)				25 (0)			
Mean (SD)	12.6 (5.44)	8.7 (5.56)				10.4 (4.04)			
Range	2.0, 24.0	2.0, 18.0				11.0			
						3.0, 16.0			
Sex, n (%)			0.37[b]				0.62[b]		
Female	5 (31.3%)	19 (48.7%)				14 (56.0%)			
Male	11 (68.8%)	20 (51.3%)				11 (44.0%)			
Missing	2	8				0			
Total MK in the lung			0.001[a]	<0.001[c]	0.004[c]		0.80[a]	0.92[c]	0.14[c]
N (Missing)	9 (9)	22 (25)				10 (15)			
Mean (SD)	3.6 (2.42)	1.5 (0.91)				1.5 (0.49)			
Range	1.1, 8.3	0.0, 3.8				0.8, 2.2			
Immature MK in the lung	22 (25)	9 (9)	<0.001[a]	<0.001[c]	<0.001[c]		0.70[a]	0.48[c]	0.01[c]
N (Missing)	0.7 (0.84)	3.4 (2.53)				10 (15)			
Mean (SD)	0.0, 3.6	1.0, 8.3				0.8 (0.39)			
Range	22 (25)	9 (9)				0.2, 1.4			
Mature MK in the lung	22 (25)	9 (9)	0.007[a]	0.009[c]	0.02[c]		0.37[a]	0.43[c]	0.72[c]
N (Missing)	0.9 (0.59)	0.3 (0.42)				10 (15)			
Mean (SD)	0.0, 2.3	0.0, 1.2				0.7 (0.36)			
Range	22 (25)	9 (9)				0.2, 1.2			
Severity of lung inflammation, n (%)			>0.99[b]	0.85[d]	0.86[d]		0.27[b]	0.08[d]	0.34[d]
0	10 (27.0%)	3 (25.0%)				9 (50.0%)			

Table 1: Comparison of age, sex, and histological parameters between *Gata1*^{low} mice vs WT and *Gata1*^{low} mice vs P-sel^{null}Gata1^{low}

	Gata1^{low} (n=47)	WT (n=18)	Unadjusted p-value	Age-adjusted p-value	Sex-adjusted p-value	P-sel^{null}Gata1^{low} (n=25)	Unadjusted p-value	Age-adjusted p-value	Sex-adjusted p-value
1	11 (29.7%)	4 (33.3%)				4 (22.2%)			
2 or 3	16 (43.2%)	5 (41.7%)				5 (27.8%)			
Missing	10	6				7			
Semiquantitative fibrosis, n (%)			0.01[b]	0.02[d]	0.001[d]		0.009[b]	0.01[d]	<0.001[d]
0	8 (27.6%)	8 (66.7%)				12 (66.7%)			
1	9 (31.0%)	4 (33.3%)				5 (27.8%)			
2 or 3	12 (41.4%)	0 (0.0%)				1 (5.6%)			
Missing	18	6				7			
Quantitative fibrosis			0.006[a]	0.01[c]	0.002[c]				
N (Missing)	29 (18)	12 (6)				18 (7)	0.01[a]	0.04[c]	0.002[c]
Mean (SD)	12.8 (11.56)	3.0 (3.10)							
Range	0.0, 45.1	0.0, 9.0							

[a]Equal variance two sample t-test p-value; [b]Fisher's exact p-value; [c]Parameter p-value from multiple linear regression with age or sex as covariate;[d]Parameter p-value from ordinal logistic regression with age or sex as covariate.

Figure 1

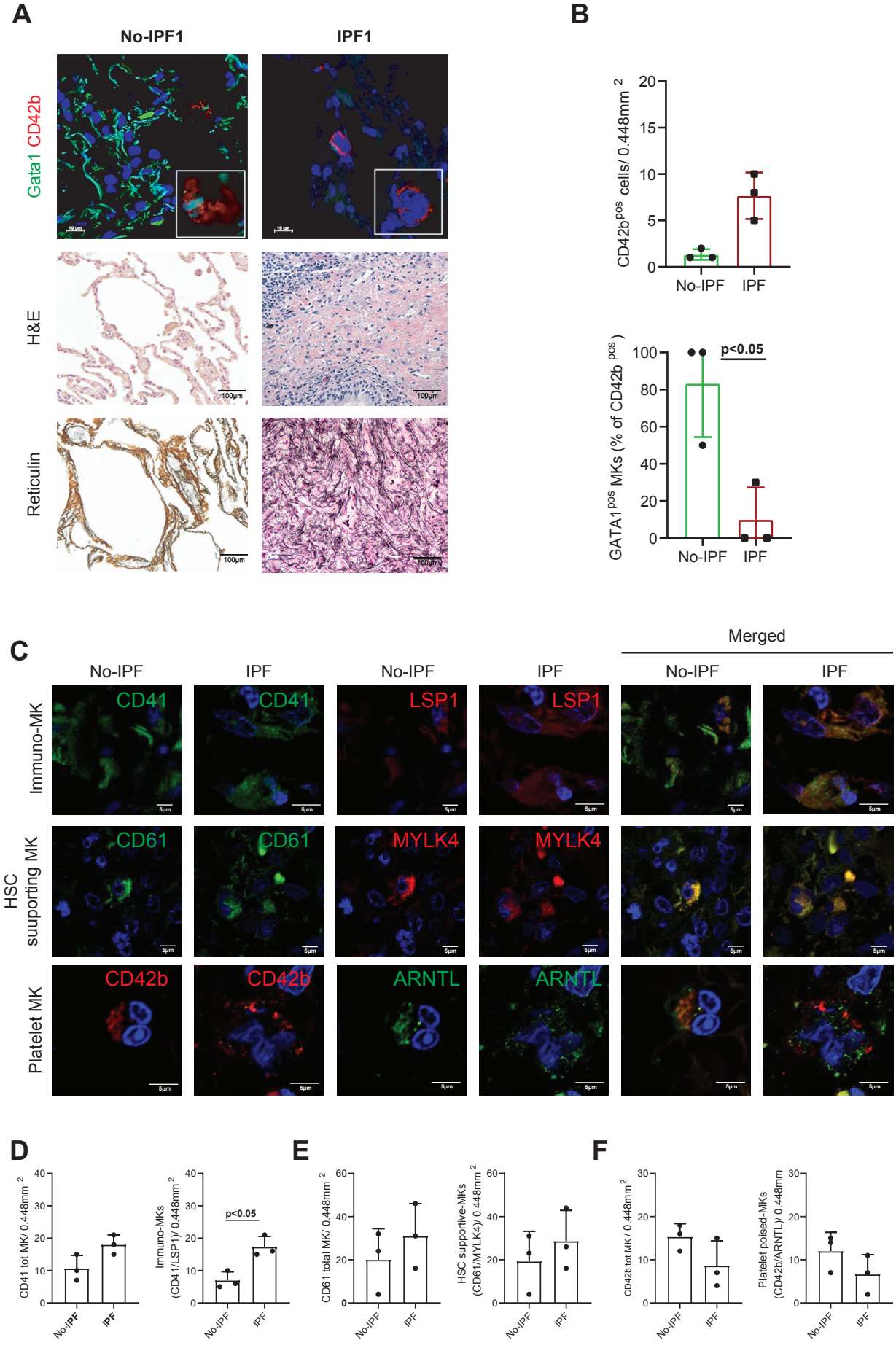
A
No-IPF1
IPF1
Gata1 CD42b
H&E
Reticulin
B
CD42b pos cells/ 0.448mm 2
No-IPF
IPF
GATA1 pos MKs (% of CD42b pos)
p<0.05
C
Merged
No-IPF
IPF
Immuno-MK
HSC suuporting MK
Platelet MK
CD41
LSP1
CD61
MYLK4
CD42b
ARNTL
D
CD41 tot MK/ 0.448mm 2
Immuno-MKs (CD41/LSP1)/ 0.448mm 2
E
CD61 total MK/ 0.448mm 2
HSC supportive-MKs (CD61/MYLK4)/ 0.448mm 2
F
CD42b tot MK / 0.448mm 2
Platelet poised-MKs (CD42b/ARNTL)/ 0.448mm

Figure 2

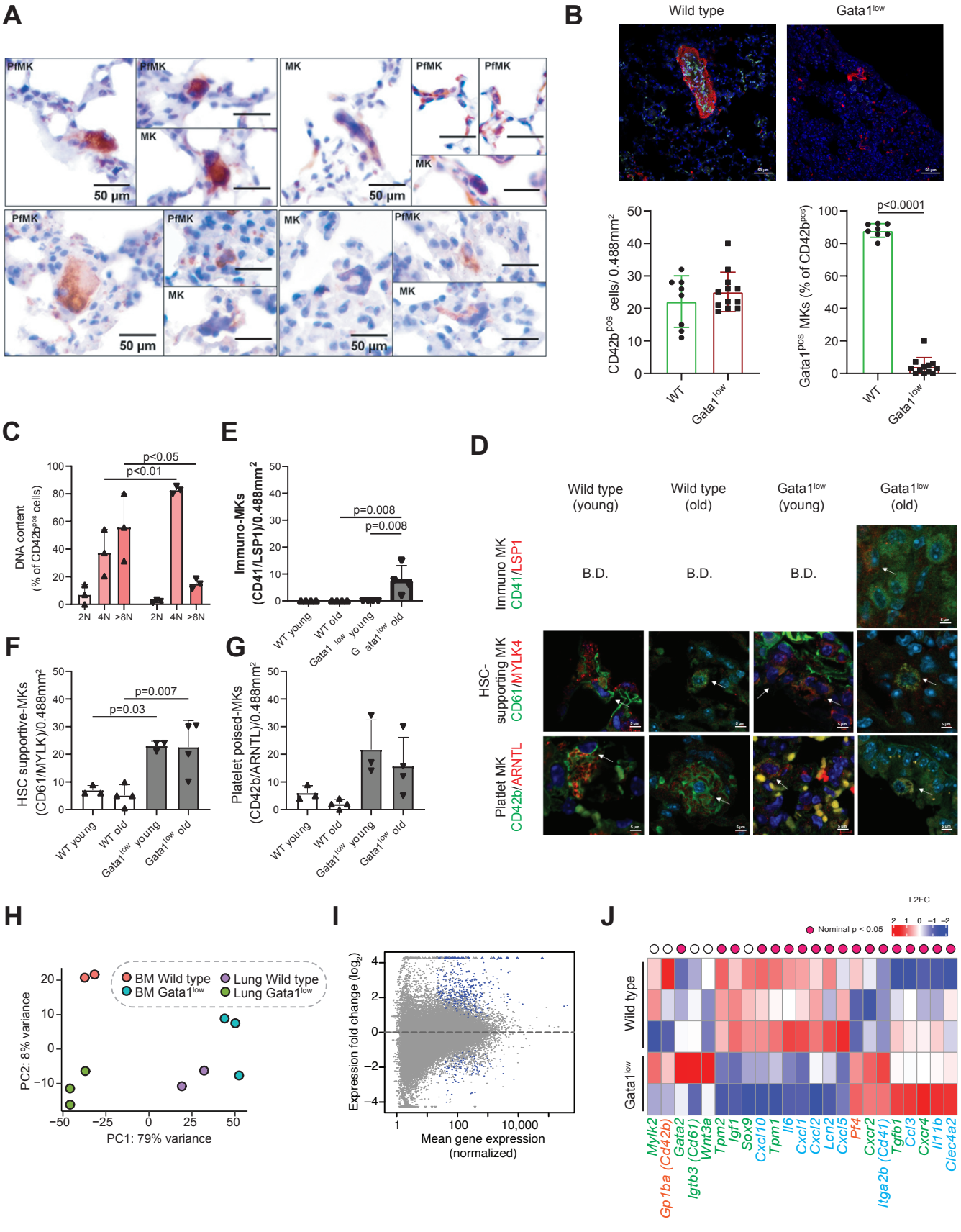
A
PfMK
MK
50 µm
B
Wild type
Gata1low
CD42bpos cells/ 0.488mm2
Gata1pos MKs (% of CD42bpos)
p<0.0001
WT
Gata1low
C
DNA content (% of CD42bpos cells)
p<0.05
p<0.01
2N 4N >8N
E
Immuno-MKs (CD41/LSP1)/0.488mm2
p=0.008
p=0.008
WT young
WT old
Gata1 low young
G ata1low old
D
Wild type (young)
Wild type (old)
Gata1low (young)
Gata1low (old)
Immuno MK CD41/LSP1
B.D.
HSC-supporting MK CD61/MYLK4
Platlet MK CD42b/ARNTL
F
HSC supportive-MKs (CD61/MYLK)/0.488mm2
p=0.007
p=0.03
G
Platelet poised-MKs (CD42b/ARNTL)/0.488mm2
H
BM Wild type
BM Gata1low
Lung Wild type
Lung Gata1low
PC2: 8% variance
PC1: 79% variance
I
Expression fold change (log2)
Mean gene expression (normalized)
J
L2FC
Nominal p < 0.05
Wild type
Gata1low
Mylk2
Gp1ba (Cd42b)
Gata2
Itgb3 (Cd61)
Wnt3a
Tpm2
Igf1
Sox9
Cxcl10
Tpm1
Il6
Cxcl1
Cxcl2
Lcn2
Cxcl5
Pf4
Cxcr2
Itga2b (Cd41)
Tgfb1
Ccl3
Cxcr4
Il11b
Clec4a2

Figure 3

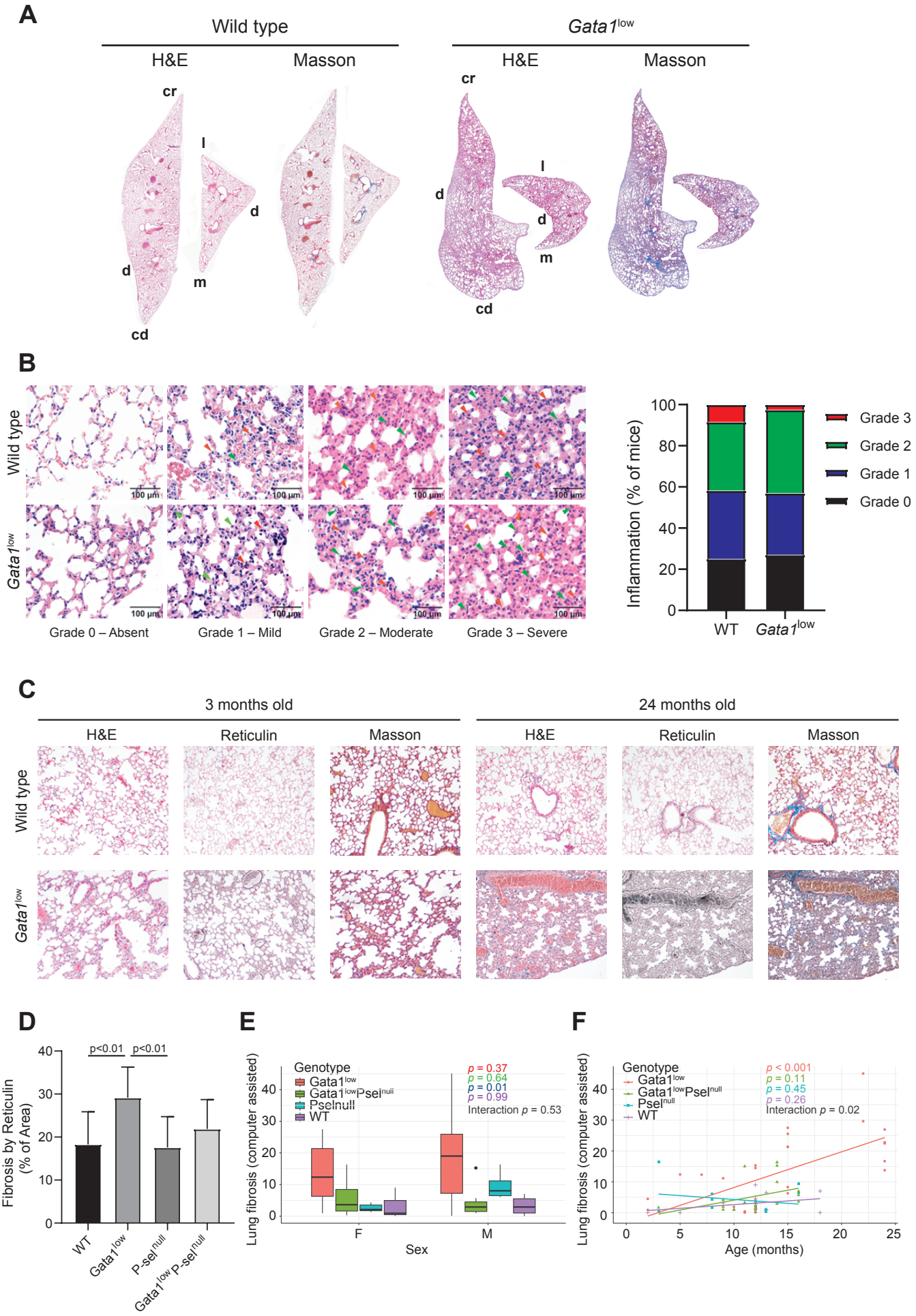
A
Wild type
Gata1low
H&E
Masson
H&E
Masson
cr
l
d
d
m
cd
cr
d
l
d
m
cd
B
Wild type
Gata1low
100 µm
Grade 0 – Absent
Grade 1 – Mild
Grade 2 – Moderate
Grade 3 – Severe
Inflammation (% of mice)
100
80
60
40
20
0
WT
Gata1low
Grade 3
Grade 2
Grade 1
Grade 0
C
3 months old
24 months old
H&E
Reticulin
Masson
H&E
Reticulin
Masson
Wild type
Gata1low
D
Fibrosis by Reticulin (% of Area)
p<0.01
p<0.01
40
30
20
10
0
WT
Gata1low
P-selnull
Gata1low P-selnull
E
Lung fibrosis (computer assisted)
Genotype
Gata1low
Gata1lowPselnull
Pselnull
WT
p = 0.37
p = 0.64
p = 0.01
p = 0.99
Interaction p = 0.53
F
Lung fibrosis (computer assisted)
Genotype
Gata1low
Gata1lowPselnull
Pselnull
WT
p < 0.001
p = 0.11
p = 0.45
p = 0.26
Interaction p = 0.02
Age (months)

Figure 4

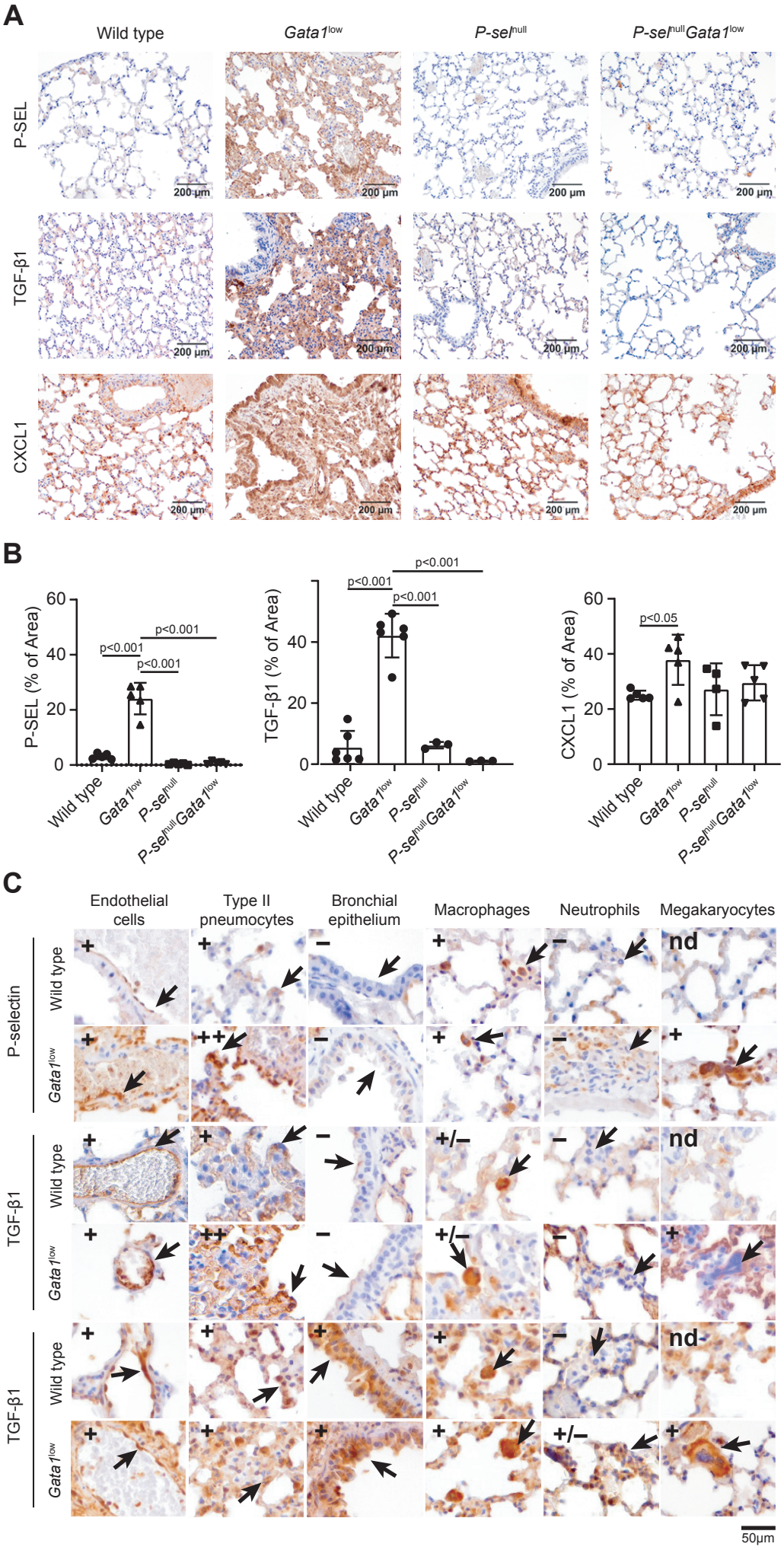
A
Wild type
Gata1low
P-selnull
P-selnullGata1low
P-SEL
TGF-β1
CXCL1
200 µm
B
P-SEL (% of Area)
TGF-β1 (% of Area)
CXCL1 (% of Area)
p<0.001
p<0.05
Wild type
Gata1low
P-selnull
P-selnullGata1low
C
Endothelial cells
Type II pneumocytes
Bronchial epithelium
Macrophages
Neutrophils
Megakaryocytes
P-selectin
TGF-β1
nd
50µm

Figure 5

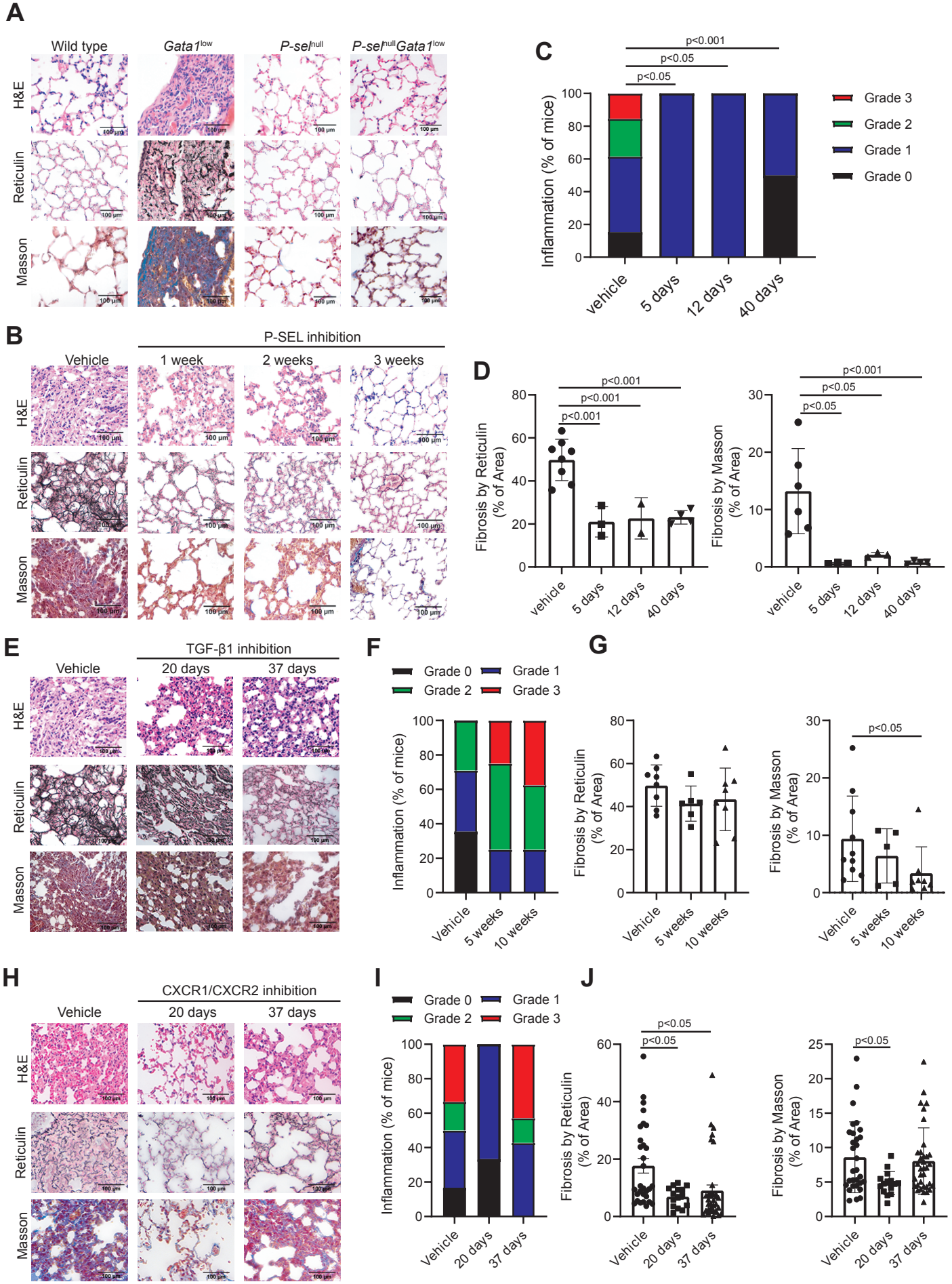
A
Wild type
Gata1low
P-selnull
P-selnullGata1low
H&E
Reticulin
Masson
B
P-SEL inhibition
Vehicle
1 week
2 weeks
3 weeks
C
p<0.001
p<0.05
p<0.05
Inflammation (% of mice)
Grade 3
Grade 2
Grade 1
Grade 0
vehicle
5 days
12 days
40 days
D
Fibrosis by Reticulin (% of Area)
Fibrosis by Masson (% of Area)
E
TGF-β1 inhibition
Vehicle
20 days
37 days
F
Grade 0
Grade 1
Grade 2
Grade 3
Vehicle
5 weeks
10 weeks
G
H
CXCR1/CXCR2 inhibition
I
J

Figure 6

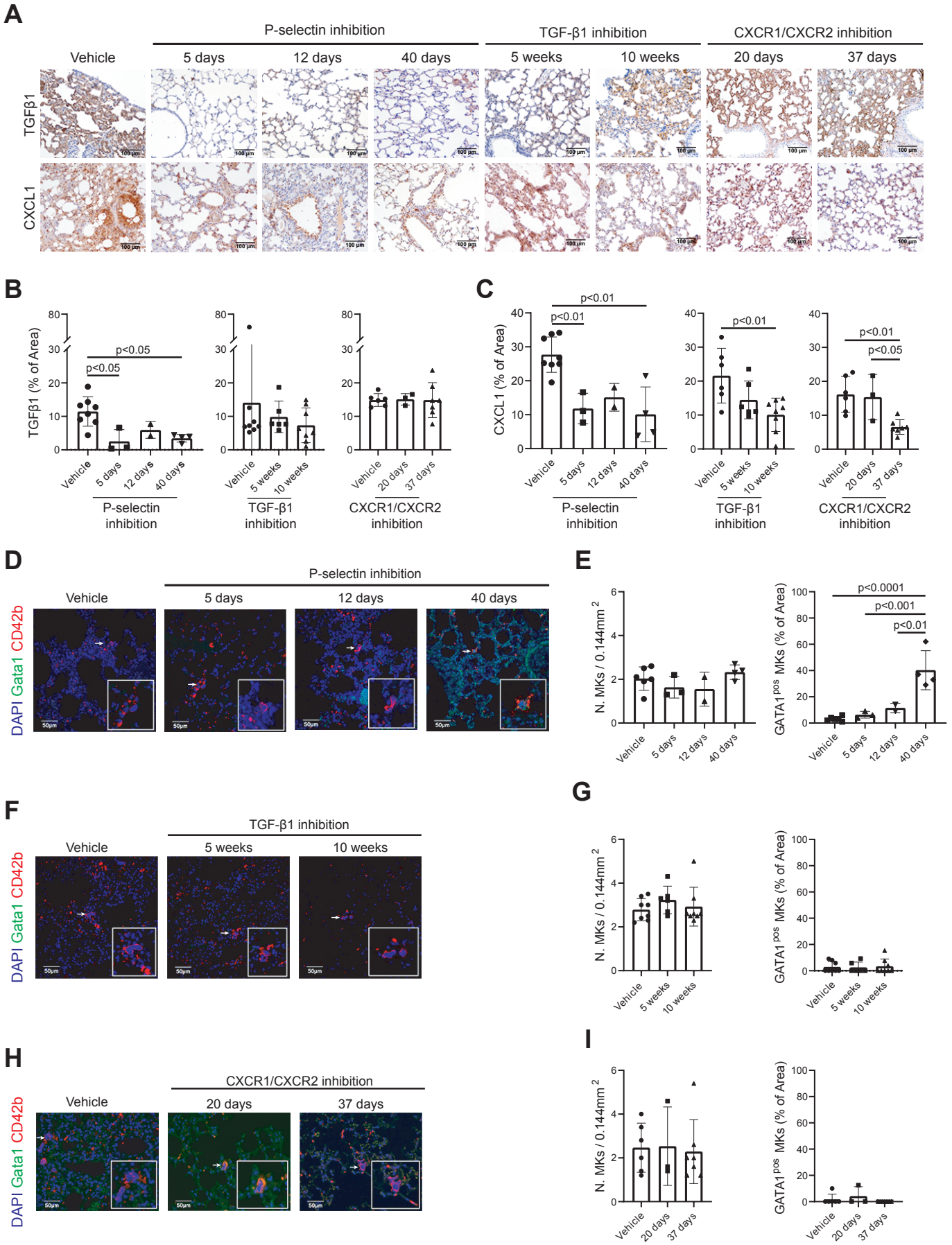
A
P-selectin inhibition
TGF-β1 inhibition
CXCR1/CXCR2 inhibition
Vehicle
5 days
12 days
40 days
5 weeks
10 weeks
20 days
37 days
TGFβ1
CXCL1
B
TGFβ1 (% of Area)
p<0.05
p<0.05
Vehicle
5 days
12 days
40 days
P-selectin inhibition
5 weeks
10 weeks
TGF-β1 inhibition
20 days
37 days
CXCR1/CXCR2 inhibition
C
CXCL1 (% of Area)
p<0.01
p<0.01
p<0.01
p<0.01
p<0.05
D
DAPI Gata1 CD42b
E
N. MKs / 0.144mm 2
GATA1 pos MKs (% of Area)
p<0.0001
p<0.001
p<0.01
F
G
H
I